Detection of superparamagnetic nanobeads with GMR technology for biosensor applications

Verheyden, K.

Award date:
2003

Nat.Lab. Technical Note 2003/127

Date of issue: 04/2003

Detection of superparamagnetic nanobeads with GMR technology for biosensor applications

K. Verheyden

Title: Detection of superparamagnetic nanobeads with GMR technology for biosensor applications

Author: K. Verheyden

Reviewers: Menno W.J. Prins (menno.prins@philips.com), Reinder Coehoorn

Technical Note: 2003/127

Project: Biosensors

Customer: Company Research

Keywords: Biosensor, molecular diagnostics, GMR, superparamagnetic beads, nanobeads

Abstract: In biological and bio-medical applications it is important to determine low molecular concentrations for a wide range of different molecules. The standard detection method uses fluorescent labels, with a detection limit between 0.1 and 1 label per μm^2. We want to develop a method that is at least 100 times better than fluorescence. We investigated a biosensor based on Giant MagnetoResistance (GMR) sensors and superparamagnetic nanoparticles as labels. In this report we explain how the biosensor works and what signal we expect for surface concentrations and bulk concentrations. It is shown experimentally that we can measure nanobeads. We measured signals of the order of microvolts for beads with a size of 50 nm and 130 nm. Estimations show that our sensor with a few modifications may be able to resolve bead concentrations of $2\ 10^{-4}$ beads per μm^2.

The research work was performed in the traineeship period 15.04.2002-15.03.2003.

Conclusions: After improving the set-up and replacing the photoresist with silicon nitride, we experimentally demonstrated that we can measure nanobeads. This measured voltage has bulk and surface components. The surface component is bigger for 130 nm beads than for 50 nm beads, due to better adhesion of bigger particles. It is also shown experimentally that the signal increases with particle concentration.

We can estimate the detection limit for our sensor with three realistic modifications: a 1000 μm long GMR stripe instead of 100 μm, a GMR stack that has a 4 times higher sensitivity and an external magnetic field of 80 kA/m. With these modification we may be able to measure $2 \cdot 10^{-4}$ particles per μm^2. Calculations and experiments are to be performed for concentrations below 0.5 beads per μm^2.

Contents

1. Introduction

Early detection is very important in biological and bio-medical applications. Important examples are oncology, infectious diseases, food diagnostics, etc. Early detection requires very sensitive measurements of a wide range of bio-molecules, for example proteins and nucleic acids. To measure low concentrations in body fluids, such as blood, we are developing a biosensor. A biosensor is an analytical device that integrates a biological element with a signal transducer (see Figure 1.1). This example sketches a sandwich assay. The biological element, for example antibodies, is a layer of capture molecules for specific interaction with the target. Biochips measure many targets at the same time, this is called multiplexing or lab on a chip. The perfect biosensor should feature a low detection limit, high sensitivity, be quantitative and fast while maintaining a low production cost. Biosensor detection principles can be electrical, magnetic, optical, or mechanical. This depends on the label which is used. The standard detection principle is optical, and has a detection limit of between 0.1 and 1 fluorescent molecule per square micrometer.

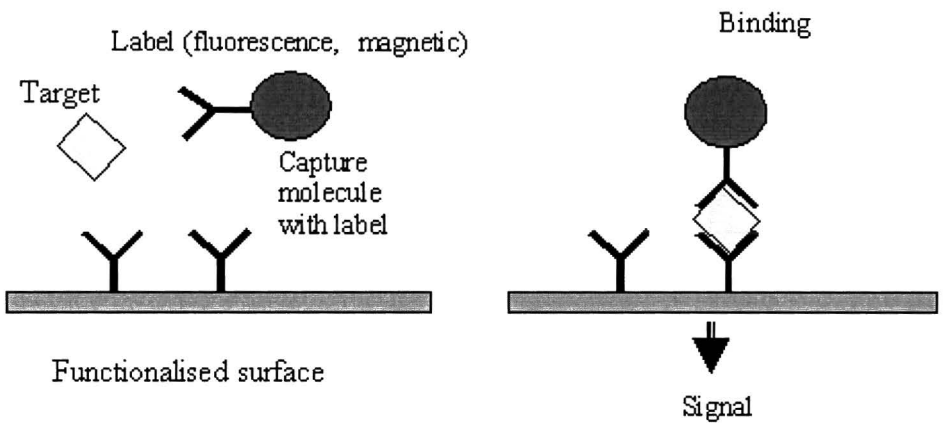

Figure 1.1: Scheme of a sandwich assay[1]. On the left capture molecules are immobilised on the surface and, target and capture molecule with label in the bulk. On the right binding of the target with the capture molecules occurs.

Our goal is to outperform fluorescent detection by at least two orders of magnitude. In this report we will look at a magnetic detection principle using Giant Magneto Resistance (GMR) and superparamagnetic nanobeads. A GMR-stripe consist of layers of magnetically different material which give a resistance change response under magnetic fields. Biological materials are generally not magnetic so the background signal during operation is low. In our magnetic biosensor we use a GMR-layer which is a sensitive layer for magnetic fields.

The work of this report is a continuation of the work of Michael Baumgartner [2]. Michael Baumgartner investigated the first chips and built an experimental set-up to measure the chips. In this report, we will describe several modifications of the chip and

of the experimental set-up and we will experimentally demonstrate that magnetic nanoparticles can be detected with the GMR biochip.

In Chapter 2 we will explain the principle of the biosensor and also some calculations and formulae, while in chapter 3 the experimental set-up is described. The experiments are posted in chapter 4 as well as the analysis and discussion. Finally the conclusions and recommendations are given in chapter 5.

This technical note represents the work Kurt Verheyden performed during his training at Philips Research Eindhoven in the Integrated Device Technology Group (15.04.2002 – 28.02.2003). During this training he achieved his master thesis in physics at the Technical University of Eindhoven. This training was carried out under the supervision of Dr. ir. M.W.J. Prins (Philips) and Prof. Dr. R. Coehoorn (Philips/Technical University Eindhoven).

2. Theory and calculations

In this chapter we will explain the concepts of the magnetic biosensor, and explain how it is possible to measure low concentrations.

2.1. Introduction

One possible type of biosensor that allows magnetic detection is a sandwich assay (see Figure 1.1). There is a chemical reaction between antigen (target) and antibody [1]:

$$[Ag]+[Ab] \underset{k_d}{\overset{k_a}{\rightleftharpoons}} [Ag+Ab], \qquad (2.1)$$

where $[Ag]$ is the concentration of the antigen, $[Ab]$ is the concentration of the antibody and $[Ag + Ab]$ is the concentration of the complex of antibody and antigen. k_a is the reaction rate to form the complex $[Ag + Ab]$ from $[Ag]$ and $[Ab]$. k_d is the reaction rate from the complex $[Ag + Ab]$ to form $[Ag]$ and $[Ab]$. There is an equilibrium in this reaction between antibody and antigen which is described by:

$$K_{eq} \equiv \frac{k_a}{k_d} = \frac{[Ag+Ab]}{[Ag][Ab]} \qquad (2.2)$$

A normal value of the equilibrium constant, K_{eq}, is between 10^6 and 10^{12} l/mole. Antibodies for which $K_{eq} < 10^9$ are not useful for biosensors, because a too high concentration $[Ag]$ is needed to form the complex $[Ag + Ab]$ [1]. We define the fraction f as:

$$f \equiv \frac{[Ag+Ab]}{[Ab]+[Ag+Ab]} = \frac{1}{\frac{1}{K_{eq}[Ag]}+1} \qquad (2.3)$$

In Figure 2.1 we see the fraction f plotted against $[Ag]$ for different values of K_{eq}. We calculate that with a value of $K_{eq} = 10^{12}$ l/mol and $[Ag] = 10^{-15}$ mol/l (=femtomolar) f = 0.001. If we assume that we have 1000 antibodies per square micrometer, we have 1 bound antigen per square micrometer. In §2.6 we will see that this is a measurable quantity. It is worth noting that we just calculated the surface concentration at infinite time. It can take a very long time to reach equilibrium for low target concentrations, due to the limited diffusion speed of bio-molecules. In practical test, the surface concentration is a few orders of magnitude lower than the values at equilibrium [1].

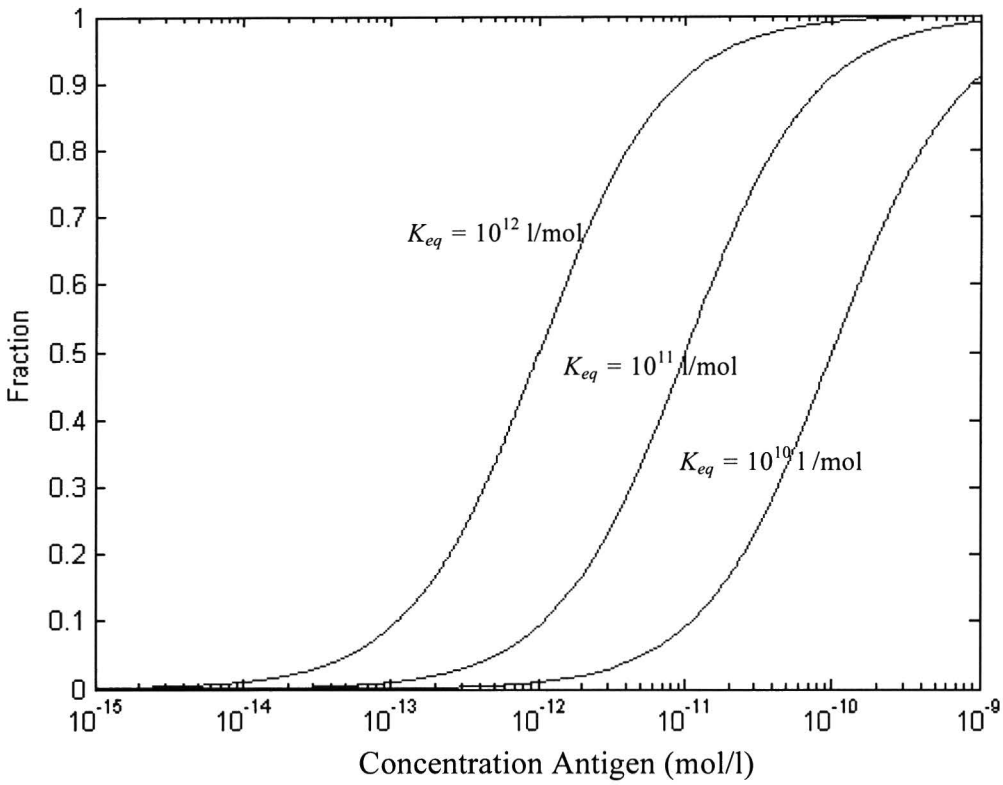

Figure 2.1: Fraction versus concentration of antigen for different values of K_{eq}.

2.2. Giant MagnetoResistance elements

The Giant-Magneto Resistance (GMR) effect is rather new but has already found many practical applications, for example in read heads for magnetic storage devices, positioning systems or magnetic tape recording [4]. It is also proposed for use in magnetic field sensors and in biosensors [3]. The most important advantages it has as compared to other low magnetic field detection methods are low power consumption, easy fabrication on a micrometer scale, low hysteresis, low cost and a high sensitivity. In view of these characteristics we chose a GMR material for our biosensor [4].

2.2.1. The GMR effect

A GMR material is a material in which the resistance depends on the angle between the magnetisation directions at different locations in the material. A GMR material can have several layer structures, as shown in Figure 2.2. The GMR effect is caused by spin-dependent scattering of electrons in ferromagnetic layers or in ferromagnetic/non-magnetic interfaces. The GMR effect will be explained for the case of an exchange biased spin-valve (Figure 2.2 b). We have a pinned layer in which magnetic orientation would not change in normal magnetic fields and we have a free layer which follows the direction of the in-plane magnetic field almost completely. This means that the GMR

materials is sensitive to in-plane fields and insensitive to fields perpendicular to the stripe. The spacer layer is used to separate the free layer and pinned layer. When the free layer has an opposite direction to the pinned layer the resistance is maximum, and for the parallel direction it is minimum. To summarise, the resistance of a GMR material is dependent on the in-plane magnetic field . In Figure 2.3 the resistance is plotted against the magnetic field. In the biosensor we will use an exchange-biased Artificial Anti Ferromagnetic (AAF) pinned layer (Appendix C) because of higher effective pinning field and better thermal stability (Figure 2.2c).

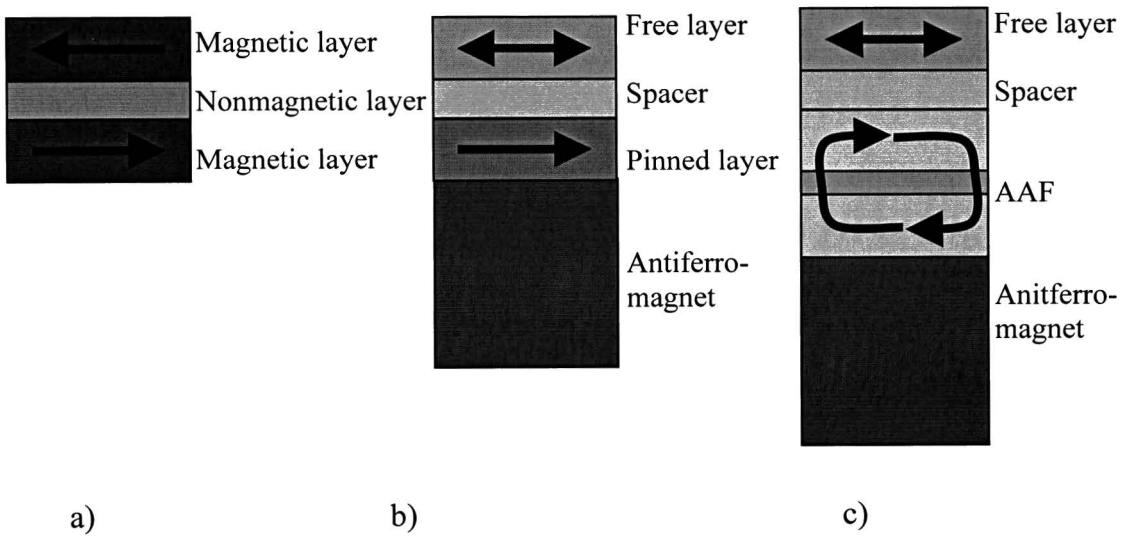

Figure 2.2: Different GMR stacks a) antiferromagnetically coupled layer, b) exchange-biased spin-valve, c) exchange-biased spin-valve with an AAF pinnend layer [2].

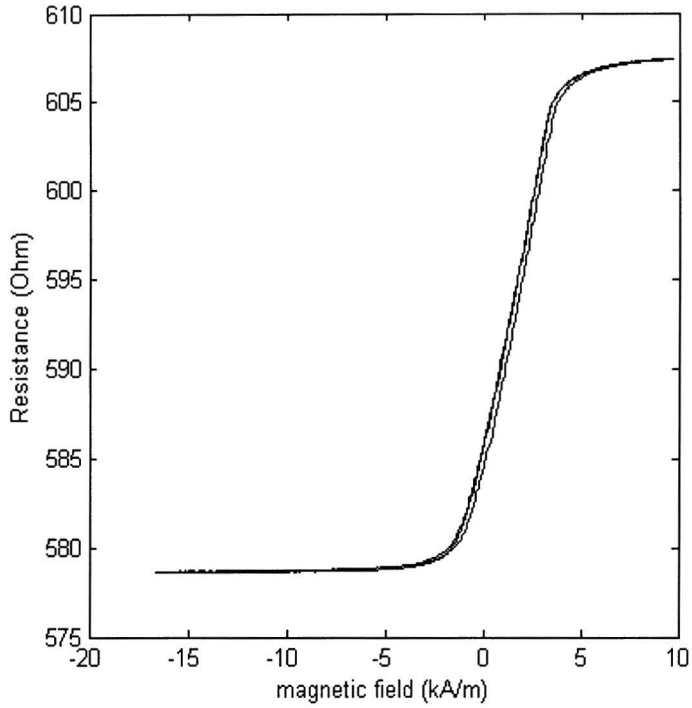

Figure 2.3: AAF GMR resistance (layer composition in Appendix C) versus magnetic field with an R_{sh} =17.36 Ω and MR_{ratio} =4.9 %.

2.2.2. GMR characteristics

The sensitive field range of the GMR material is the field range in which the free magnetic layer reverses from parallel to anti-parallel magnetisation or vice versa. The width of this field interval is called the switch field range, ΔH_s. In Figure 2.3 it can be observed that the sensitive field interval is around zero magnetic field. To characterise the GMR element usually the MR_{ratio} and the sheet resistance, R_{sh}, are given, which are defined as:

$$MR_{ratio} = \frac{\Delta R}{R_{\min}} = \frac{R_{\max} - R_{\min}}{R_{\min}} \qquad (2.4)$$

$$R_{sh} = \frac{R * w}{l}, \qquad (2.5)$$

where w is the width and l is the length of the GMR. Also very important is the sensitivity:

$$s = \frac{\Delta R}{\Delta H_s} \qquad (2.6)$$

The MR_{ratio} (2.4) and s (2.6) for the GMR in Figure 2.3 is 0.049 and 0.0053 Ωm/A respectively. The sheet resistance, R_{sh}=17.36 Ω

2.3. Sensor concept

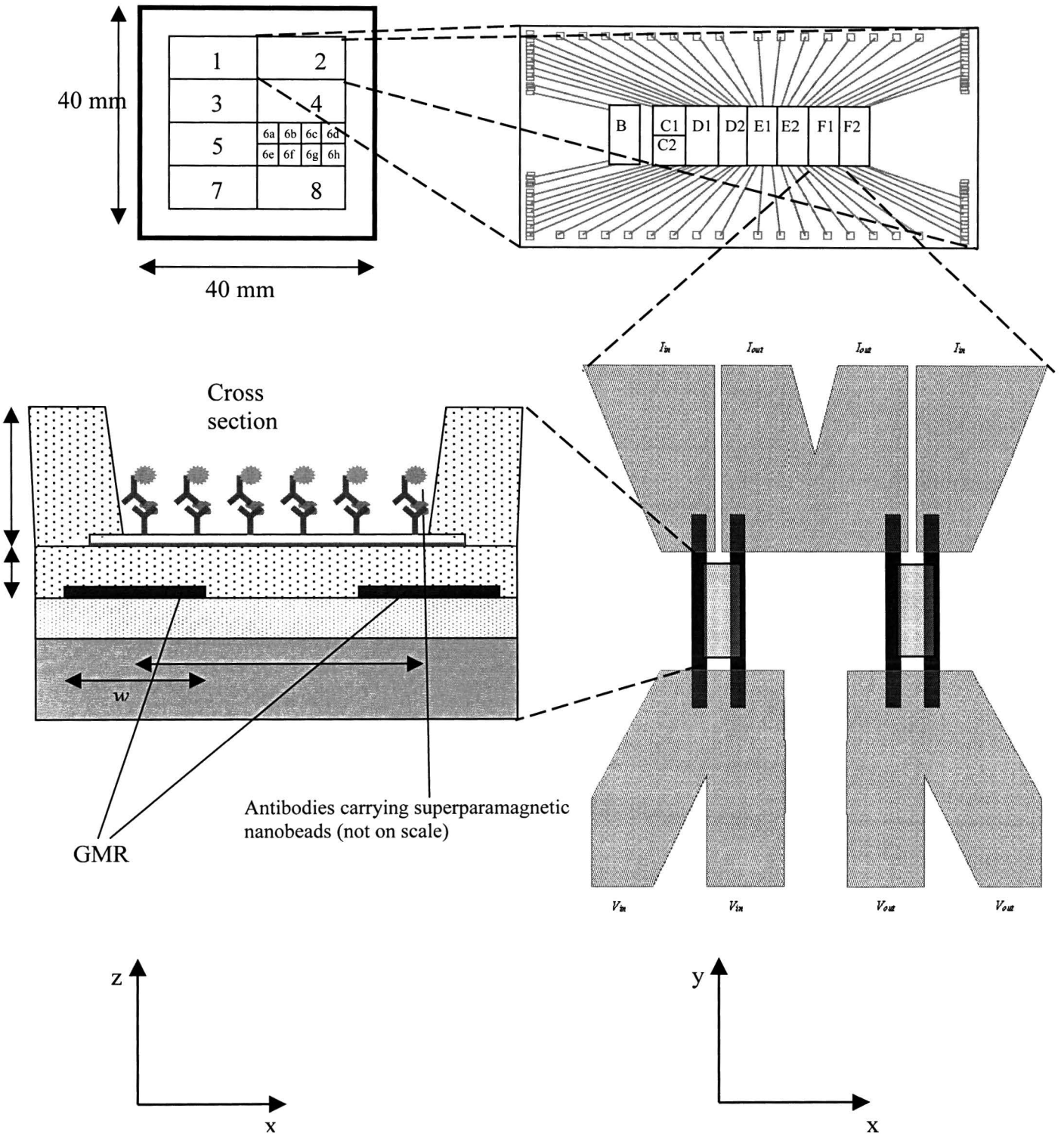

Figure 2.4: Schematic overview of biochip.

In Figure 2.4 a schematic overview is shown. The biosensor is produced on a 40 by 40 mm wafer where 7 biosensors (1,2,3,4,5,7,8) and 4 noise measuring sensors (6a,b,c,d) are located on. Each biosensor contains 8 structures to measure target concentration [2]. Each structure is a Wheatstone bridge (see §2.3.4) and each wheatstone bridge exits out of 2 pairs of sensor elements. Each sensor element has an area where the antibodies can be attached on. There is a channel and below the edges of the channel the GMR-stripes are located.

On top of the biochip a flow cell (see §3.1.3) is mounted, through this flow cell target and superparamagnetic beads can be added. An external magnetic field is applied in the z-direction (Figure 2.4). The magnetic beads will give rise to a magnetic field due to the external magnetic field. This will change the resistance in the GMR-stripes and the resistance change that can detect as a change in voltage in the Wheatstone bridge.

2.3.1. Bulk solution and surface bound beads

There are two methods of using the sensor. The first is to determine the area concentration of the beads that are immobilised on the surface. This is the method we are going to use to determine target concentrations. Another way is the bulk method. This means that the beads are free to move around in the channel (Figure 2.5). Panel (a) and (b) show surface methods and (c) a bulk method. Surface should be related to target and bulk should not be related to target. The magnetic beads will give a magnetic field due to an external magnetic field *H*.

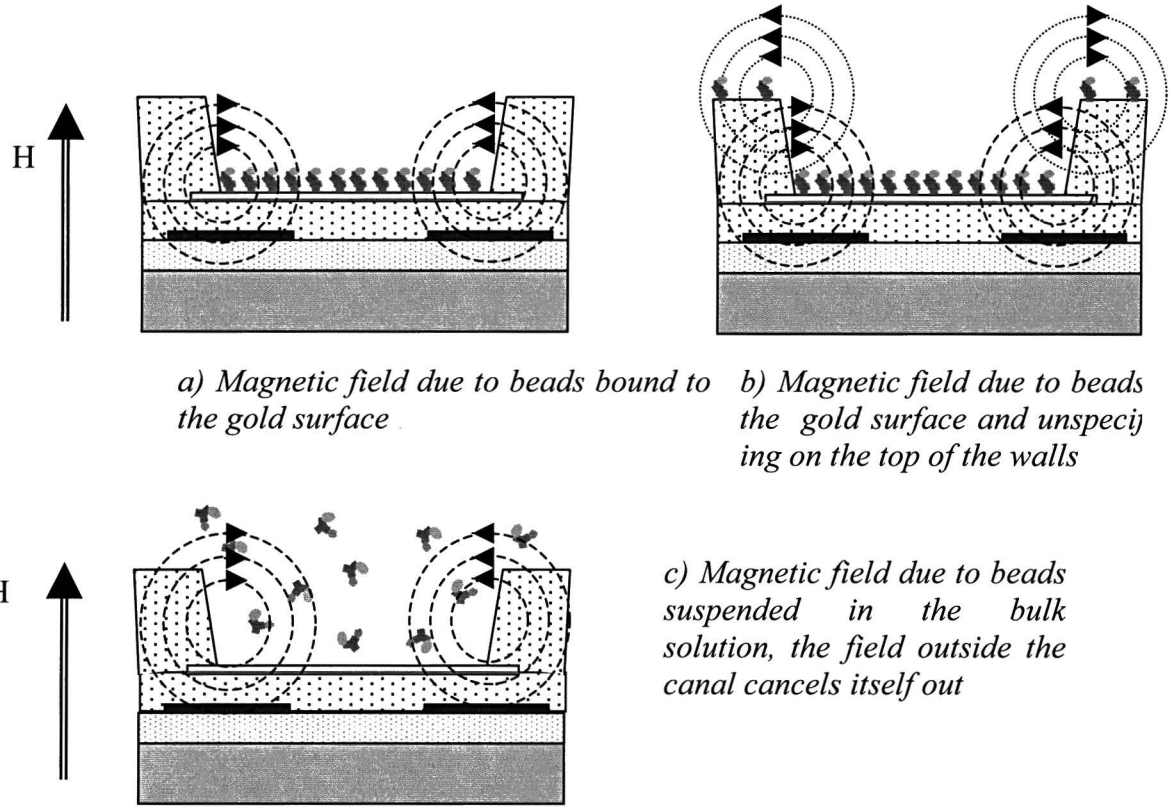

a) Magnetic field due to beads bound to the gold surface

b) Magnetic field due to beads the gold surface and unspecij ing on the top of the walls

c) Magnetic field due to beads suspended in the bulk solution, the field outside the canal cancels itself out

Figure 2.5: Magnetic field due to the magnetised beads immobilised only on the gold layer (a), on the whole chip area (b) or still mobile (c)[2].

2.3.2. Dimensions of the chip

The dimensions of a sensor element are (see Figure 2.6) t_1 = 0.5 μm, t_2 = 3 μm, w = 3 μm, W = 6 μm. W is division of the surface where the antibodies are immobilised on the gold, the length of the sensor element is 100 μm.

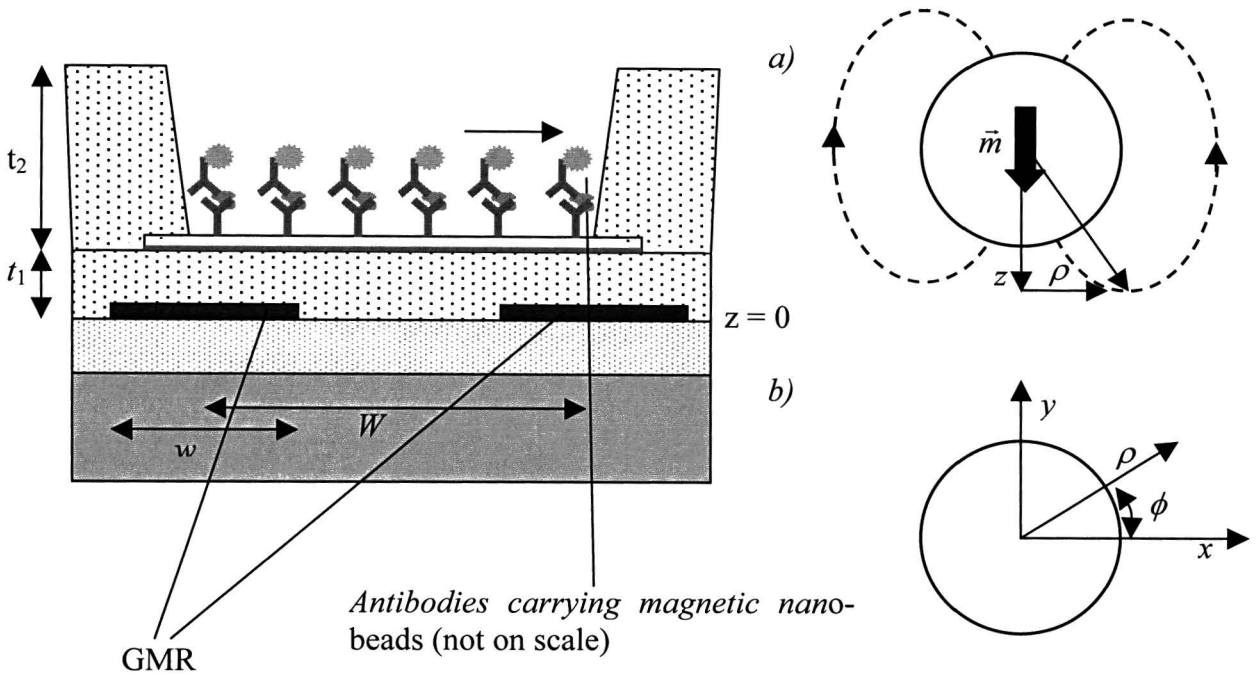

Figure 2.6: Left: cross-section through one sensor element, the nanobeads are immobilised on the gold surface. Right: Coordinate system for an enlarged nanobead relative to the sensor plane a) side view, b) top view [2].

2.3.3. Magnetic field due to magnetic beads

When an external field is applied the superparamagnetic magnetic beads, whether they are immobilised or in bulk solution, will give rise to an additional magnetic field at the edges of the sensor element. The magnetic field H of one bead can be described as a dipole at the centre of the bead. So at a certain distance r from the centre of the bead the magnetic field H will become [5]:

$$\vec{H}(\vec{r}) = \frac{3\hat{r}(\hat{r}.\vec{m}) - \vec{m}}{2\pi r^3}, \qquad (2.7)$$

where m is the magnetic moment of the bead and $\hat{r}$ is the unit vector of r. The magnetic moment $\vec{m} = m\hat{z}$ is oriented perpendicular to the plane if we apply a magnetic field perpendicular to the GMR stripe. An advantage of the GMR stripe is that it is insensitive to the out-of-plane field. The in-plane component of the field is axially symmetric and is therefore expressed in cylindrical coordinates:

$$H_\rho = \frac{3mz\rho}{2r^5\pi} \qquad (2.8)$$

with $r = \sqrt{\rho^2 + z^2}$. If we consider a layer without thickness, infinite length and semi-infinite width, the magnetic field in the x-direction at a distance z to the edge is given through:

$$H_x = \int\int \frac{3mnz\rho^2 \cos(\phi)}{2\pi\left(\sqrt{\rho^2 + z^2}\right)^5} d\rho d\phi = \frac{mn}{2\pi z} \qquad (2.9)$$

where n is the density of the particles on the surface. This is equal to the magnetic field of a current wire with current I:

$$I = mn. \qquad (2.10)$$

As we explained in § 2.2.1 the x-component of the magnetic field will give a change in the resistance of the GMR element. This field H_x is either positive or negative, in the GMR element to the right respectively to the left. The total resistance change in one GMR stripe depends on the average x-component in the stripe (Figure 2.3). If we take x = 0 in the middle of one stripe the average component is :

$$H_{x,av} = \frac{1}{\pi w} \int_{-\frac{w}{2}}^{\frac{w}{2}} \frac{It_1}{x^2 + t_1^2} dx = \frac{2mn}{\pi w} \arctan\left(\frac{w}{2t_1}\right) \qquad (2.11)$$

There are two methods to measure: bulk and surface (see Figure 2.5). There are two different structures in the surface method, one with only specific bound beads (Figure 2.5 a) and one with also non-specific bound beads (Figure 2.5 b). For the situations shown in Figure 2.5.a we can use (2.11) and for the situations shown in Figure 2.5.b we have to use:

$$H_{non-specific,x,av} = H_{x,av}(t_1) - H_{x,av}(t_2) \qquad (2.12)$$

The dimensions of our sensor structure are t_1 = 0.5 μm and t_2 = 3 μm. The presence of non-specific bound beads thus gives us a reduction in $H_{x,av}$ of 37 % when the bead concentration is as equal at t_1 and $t_1 + t_2$.

In a bulk experiment the beads will have no chemical binding to the surface. The fields of beads outside of the channel will cancel, but the beads in the channel will give rise to a magnetic field in the x-component:

$$H_{bulk,x,av} = \int_{t_1}^{t_1+t_2} \frac{2mN}{\pi w} \arctan\left(\frac{w}{2t}\right) dt =$$

$$\frac{2mN}{\pi w}\left[t \arctan\left(\frac{w}{2t}\right) + \frac{w}{4} \ln\left(\left(\frac{2t}{w}\right)^2 + 1\right)\right]_{t_1}^{t_1+t_2} = 2.24 \cdot 10^{-6}\,\text{mN} \qquad (2.13)$$

where N is the volume concentration of the beads. Our experiments will be a bulk plus non-specific bound experiment at the same time, because we are not using antibodys.

2.3.4. Wheatstone bridge

To obtain a signal around zero volt we are going to use a Wheatstone bridge (Figure 2.7). Two pairs of sensor elements can form a Wheatstone bridge configuration. All stripes have to be magnetically equal which means that the exchange bias direction has to be in the same direction. This has the advantage that they are easy to produce, with common GMR fabrication technology. The signal V_s in a Wheatstone bridge is given by:

$$V_s = I\left(\frac{R_1 - R_2 - R_3 + R_4}{4}\right) \qquad (2.14)$$

where I is the sum of the current in both arms of the bridge. For each R we can take a GMR stripe, so the left of Figure 2.7 can be connected as a Wheatstone bridge.

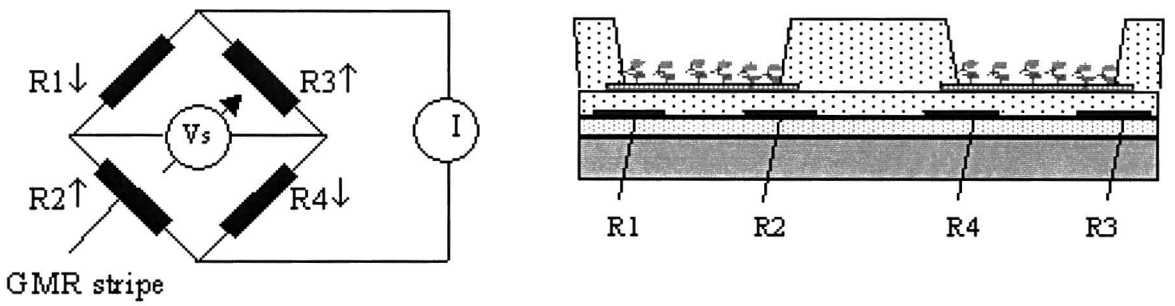

Figure 2.7: Wheatstone bridge configuration of the GMR elements [2].

The magnetic beads will give either an increment or decrement in resistance in R_1 and R_4 while it gives an decrement or increment in R_2 or R_3. So V_s becomes by using (2.6) and (2.14):

$$V_s = I\Delta R = I.s_{GMR}H_{x,av} \qquad (2.15)$$

2.4. Theory of noise

Each electronic device has noise. There are two different kinds of noise: thermal noise or white noise, and 1/f noise. Noise is expressed in S_v (voltage noise spectral density [V^2/Hz]). The voltage noise spectral density of thermal noise is given by:

$$S_v = 4k_BTR \qquad (2.16)$$

where k_B is Boltzmann constant, T is the temperature in Kelvin, and R is the resistance. We see that the thermal noise is independent of frequency. The thermal noise spectral density originates from thermal fluctuations of electrons, while 1/f noise has an origin that is not well understood. The 1/f noise is also encountered in nature, such as earthquakes, biological systems like heartbeat periods, et cetera [6]. 1/f noise can be described by the Hooge relation :

$$S_v = \frac{\alpha(H)}{Nf^{\gamma}} I^2, \qquad (2.17)$$

where the exponent γ is of order one and the total number of conduction electrons in the sample is N. The dimensionless normalizing constant α is called the Hooge constant which for magnetic materials depends on the magnetic state of the device [7].

2.5. Statistics

In this section I will give some formulas in relation with standard deviation and errors. First the formulas concerning the error will be given. For example if function $f = a \pm \Delta a$ and $g = b \pm \Delta b$ then:

$$f + g = a + b \pm (\Delta a + \Delta b), \qquad (2.18)$$

$$c * f = c * a \pm c * \Delta a, \qquad (2.19)$$

$$f.g = a.b \pm (a\Delta b + b\Delta a) \text{ and} \qquad (2.20)$$

$$\frac{f}{g} = \frac{a}{b} \pm \left(\frac{\Delta a}{b} + \frac{a\Delta b}{b^2} \right), \qquad (2.21)$$

were c = constant. These formulas will be used in §2.6.

If an experiment is performed and we have $x_1, x_2 \ldots, x_n$ measurements, the standard deviation σ is calculated by:

$$\bar{x} = \sum_i x_i \qquad (2.22)$$

$$\sigma^2 = \frac{1}{(n-1)} \sum_i (x_i - \bar{x})^2 \qquad (2.23)$$

where $\bar{x}$ is the mean of x_i. The standard deviation in the mean σ_m can also be calculated from $x_1, \ldots, x_n$:[8]

$$\sigma_m^2 = \frac{1}{n(n-1)} \sum_i (x_i - \bar{x})^2 \qquad (2.24)$$

2.6. Signal calculations

In this chapter the calculations are given for Nanomag 130 nm beads and Nanomag 50 nm beads. The beads consist of a dextrane matrix and single magnetic cores of Fe_3O_4. These beads are used in the experiments we will discuss later in the report.

The magnetic moment per g of the beads is measured by Holger Grüll in a Vibrating Sample Magnetometer (VSM)(Figure 2.8).

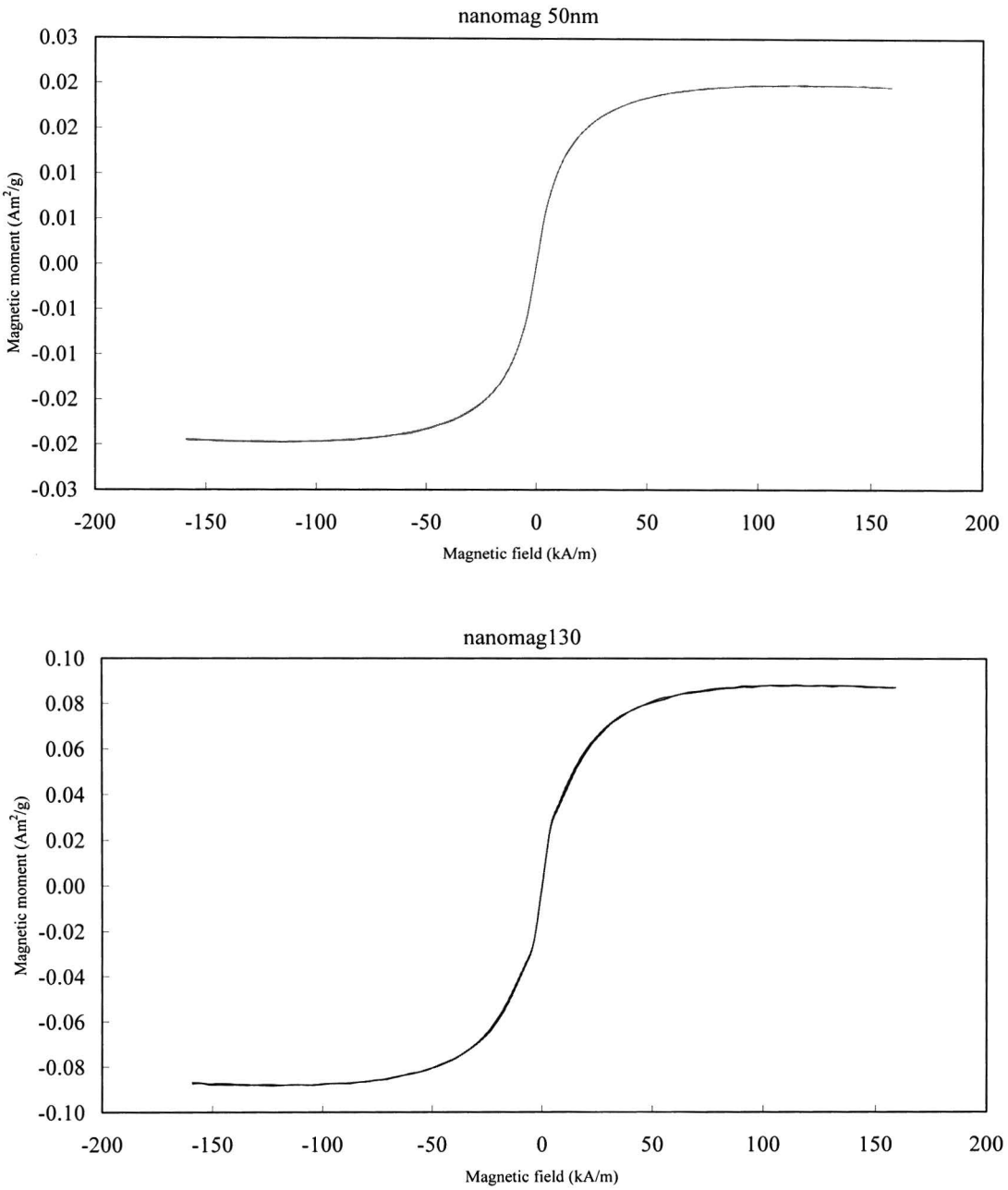

Figure 2.8: Magnetic moment versus magnetic field of 50 nm and 130 nm beads measured with the VSM.

From Figure 2.8 we can derive that the magnetic moment M at $\mu = 8 \pm 0.8$ kA/m and $\mu = 80 \pm 1$ kA/m is for the 50 nm beads:

$$M\left(8\,{}^{kA}/_{m}\right) = 9.05 \pm 0.55\,10^{-3}\ {}^{\mathrm{Am}^2}/_{\mathrm{g}} \qquad (2.25)$$

$$M\left(80\,{}^{kA}/_{m}\right) = 19.65 \pm 0.13\,10^{-3}\ {}^{\mathrm{Am}^2}/_{\mathrm{g}} \qquad (2.26)$$

The error of M is due to the of the error of the magnetic field we apply. The radius r of the beads is given by the manufacturer and the mass density ρ is estimated:

$$r = 24.0 \pm 7.6 \text{ nm} \quad (2.27)$$

$$\rho = 1300 \pm 100 \, {kg}/{m^3} \quad (2.28)$$

So the volume of one bead and the mass is by using:

$$V = 5.79 \pm 1.31 \ 10^{-23} \text{ m}^3 \quad (2.29)$$

$$mass = 7.5 \pm 2.31 \ 10^{-17} \text{ g} \quad (2.30)$$

From (2.30), (2.25) and (2.26) we can calculate the magnetic moment of 1 bead:

$$m\left(8 \, {kA}/{m}\right) = 6.8 \pm 2.5 \ 10^{-19} \text{ Am}^2 \quad (2.31)$$

$$m\left(80 \, {kA}/{m}\right) = 14.7 \pm 4.6 \ 10^{-19} \text{ Am}^2 \quad (2.32)$$

From (2.11) for the surface and (2.13) for the bulk and the dimensions that are given in §2.3.2 we can calculate $H_{x,av}$ if we use for a surface density of the beads 1 per μm^2 and for a bulk density of the beads 1 per μm^3:

$$H_{x,av,surface}\left(8 \, {kA}/{m}\right) = 1.80 \pm 0.66 \ 10^{-1} \ {A}/{m} \quad (2.33)$$

$$H_{x,av,surface}\left(80 \, {kA}/{m}\right) = 3.90 \pm 1.22 \ 10^{-1} \ {A}/{m} \quad (2.34)$$

$$H_{x,av,bulk}\left(8 \, {kA}/{m}\right) = 3.05 \pm 1.12 \ 10^{-1} \ {A}/{m} \quad (2.35)$$

$$H_{x,av,bulk}\left(80 \, {kA}/{m}\right) = 6.59 \pm 2.06 \ 10^{-1} \ {A}/{m} \quad (2.36)$$

From these values of $H_{x,av}$ and from (2.12), where $I = 10^{-3}$A and $s_{GMR} = 5 \ 10^{-3}$ Ωm/A, we can calculate the voltage signal we should measure in our Wheatstone bridge:

$$V_{surface}\left(8 \, {kA}/{m}\right) = 0.9 \pm 0.3 \, \mu V \quad (2.37)$$

$$V_{surface}\left(80 \, {kA}/{m}\right) = 2.0 \pm 0.6 \, \mu V \quad (2.38)$$

$$V_{bulk}\left(8 \, {kA}/{m}\right) = 1.5 \pm 0.6 \, \mu V \quad (2.39)$$

$$V_{bulk}\left(80 \, {kA}/{m}\right) = 3.3 \pm 1.0 \, \mu V \quad (2.40)$$

This is the voltage we expect for the 50 nm beads in the wheatstone bridge.

We also can do this for the 130 nm beads. The magnetisation of the 130 nm beads can be obtained from Figure 2.8:

$$M\left(8 \, {kA}/{m}\right) = 3.57 \pm 0.18 \ 10^{-2} \ {\text{Am}^2}/{\text{g}} \quad (2.41)$$

$$M\left(80 \, {kA}/{m}\right) = 8.65 \pm 0.02 \ 10^{-2} \ {\text{Am}^2}/{\text{g}} \quad (2.42)$$

The radius r of the beads is given by the manufacturer and the mass density ρ is estimated:

$$r = 65.0 \pm 27.6 \text{ nm} \quad (2.43)$$

$$\rho = 1300 \pm 100 \, {kg}/{m^3} \quad (2.44)$$

So the volume of one bead and the mass is:

$$V = 1.15 \pm 0.35 \ 10^{-21} \ \mathrm{m}^3 \quad (2.45)$$

$$mass = 1.50 \pm 0.57 \ 10^{-15} \ \mathrm{g} \quad (2.46)$$

From (2.46), (2.41)and (2.42)we can calculate the magnetic moment of 1 bead:

$$m\left(8 \, {kA}/{m}\right) = 5.4 \pm 2.3 \ 10^{-17} \ \mathrm{Am}^2 \quad (2.47)$$

$$m\left(80 \, {kA}/{m}\right) = 13.0 \pm 5.0 \ 10^{-17} \ \mathrm{Am}^2 \quad (2.48)$$

From (2.11)for the surface and (2.13) for the bulk and the dimensions that are given in §2.3.2 we can calculate $H_{x,av}$:

$$H_{x,av,surface}\left(8 \, {kA}/{m}\right) = 14.3 \pm 6.1 \ {\mathrm{A}}/{\mathrm{m}} \quad (2.49)$$

$$H_{x,av,surface}\left(80 \, {kA}/{m}\right) = 34 \pm 13 \ {\mathrm{A}}/{\mathrm{m}} \quad (2.50)$$

$$H_{x,av,bulk}\left(8 \, {kA}/{m}\right) = 24 \pm 10 \ {\mathrm{A}}/{\mathrm{m}} \quad (2.51)$$

$$H_{x,av,bulk}\left(80 \, {kA}/{m}\right) = 58 \pm 22 \ {\mathrm{A}}/{\mathrm{m}} \quad (2.52)$$

From these values of $H_{x,av}$ and from (2.12), where $I = 10^{-3}$A and $s_{GMR} = 5 \ 10^{-3}$ Ωm/A, we can calculate the voltage signal we should measure in our wheatstone bridge:

$$V_{surface}\left(8 \, {kA}/{m}\right) = 72 \pm 30 \, \mu\mathrm{V} \quad (2.53)$$

$$V_{surface}\left(80 \, {kA}/{m}\right) = 173 \pm 67 \, \mu\mathrm{V} \quad (2.54)$$

$$V_{bulk}\left(8 \, {kA}/{m}\right) = 121 \pm 52 \, \mu\mathrm{V} \quad (2.55)$$

$$V_{bulk}\left(80 \, {kA}/{m}\right) = 291 \pm 112 \, \mu\mathrm{V} \quad (2.56)$$

3. Experimental set-up and chip layout

In this chapter the experimental set-up for the bead experiments and for the noise experiments is explained. Further detail about the chip and chip layout is also provided in section 3 where the experiment is conducted on. The bead experiments were preformed at Philips Research Eindhoven and the noise experiments are done at the Technical University of Eindhoven.

3.1. Bead experiment

3.1.1. Bead properties

In our experiments we use two different kinds of beads, the Nanomag 50 nm and the Nanomag 130 nm. The manufacturer of the beads is Micromod Partikeltechnologie in Germany. The Nanomag 50 nm beads have radius of 24 ± 7.6 nm while the 130 nm beads have a radius of 65 ± 27 nm. The beads consist of a dextrane matrix and single magnetic cores of Fe_3O_4. It is possible to associate the bead to streptavidin which is an affinity ligand for biotin [10].

3.1.2. Chip layout

The dimensions of the chip were given in §2.3.2 along with the explanation of the Wheatstone bridge configuration. A sensor element is built from a silicon (Si) base with a silicon oxide (SiO_2). On these silicon oxide the GMR stripes are deposited (C). Above the GMR structure a thin layer of silicon nitride (Si_3N_4) is deposited to cover the GMR stripes. On this silicon nitride the gold layer used to immobilise the antibodies. Also the walls are deposited on the first layer of Si_3N_4 (Figure 3.1). These walls were first produced in a photoresist, but there was not a good adhesion of this photoresist [1] . Different baking time and different baking temperatures were used, but none resulted in satisfactory adhesion (Figure 3.2). For this reason we made the wall from Si_3N_4 which has a very good adhesion. To connect the GMR stripes we use an eight-terminal Wheatstone bridge (Figure 3.3).

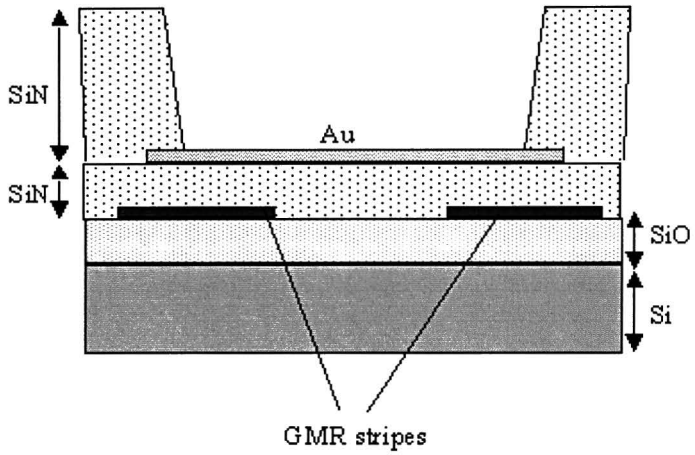

Figure 3.1: Cross-section of sensor element.

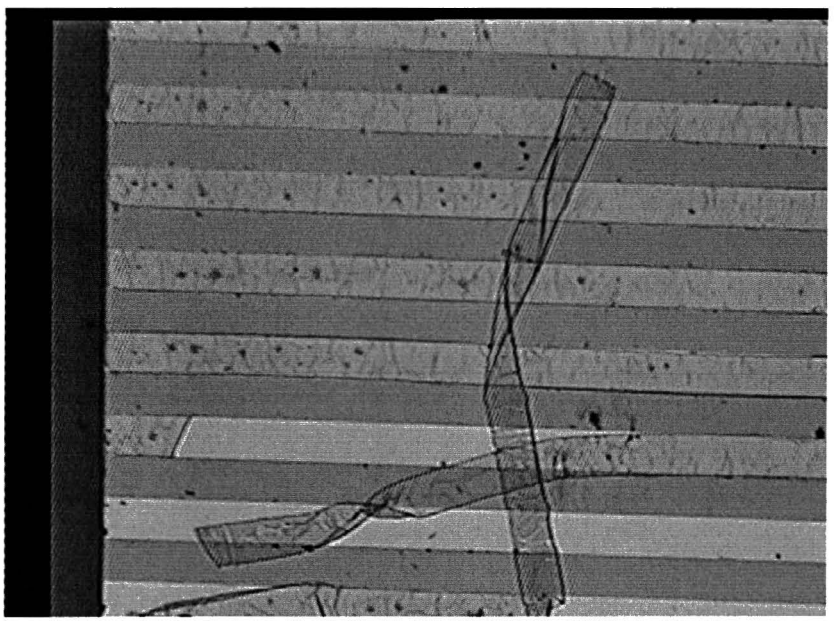

Figure 3.2: Lift-off of the photoresist.

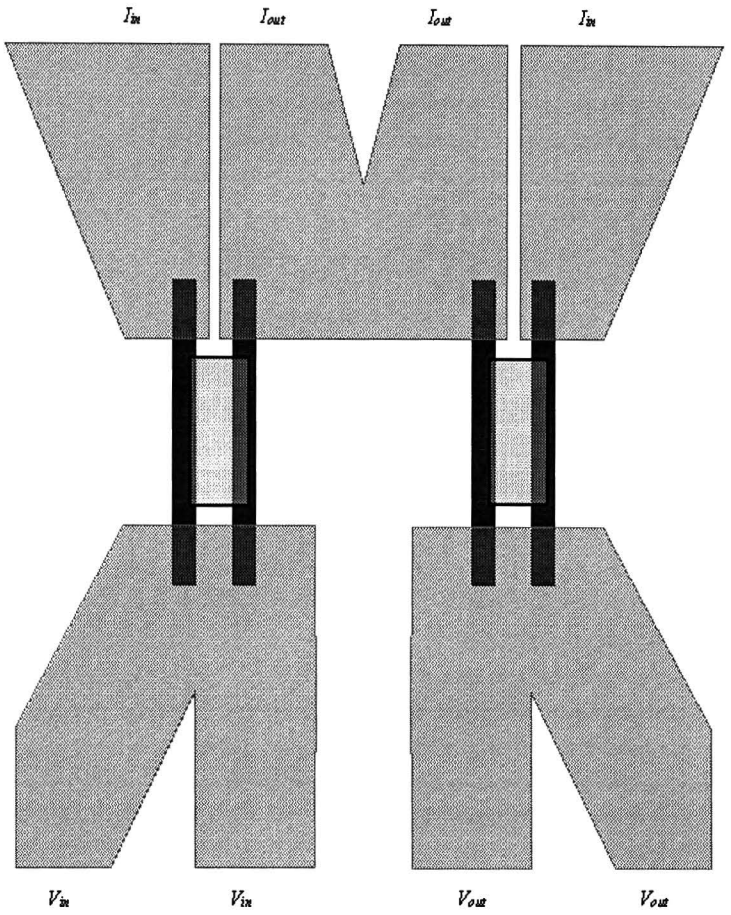

Figure 3.3: Eight-terminal Wheatstone bridge.

Sometimes it occured that a GMR-stripe changed its resistance. In Figure 3.4 you can see that not only the resistance changed but that also the properties of the GMR have changed. Pictures showed a damaged Wheatstone bridge (Figure 3.5) A possible explanation is that static electricity caused too high currents and damaged the GMR stripe. For that reason it is advisable to wear a ground connector on your wrist when handling GMR chips.

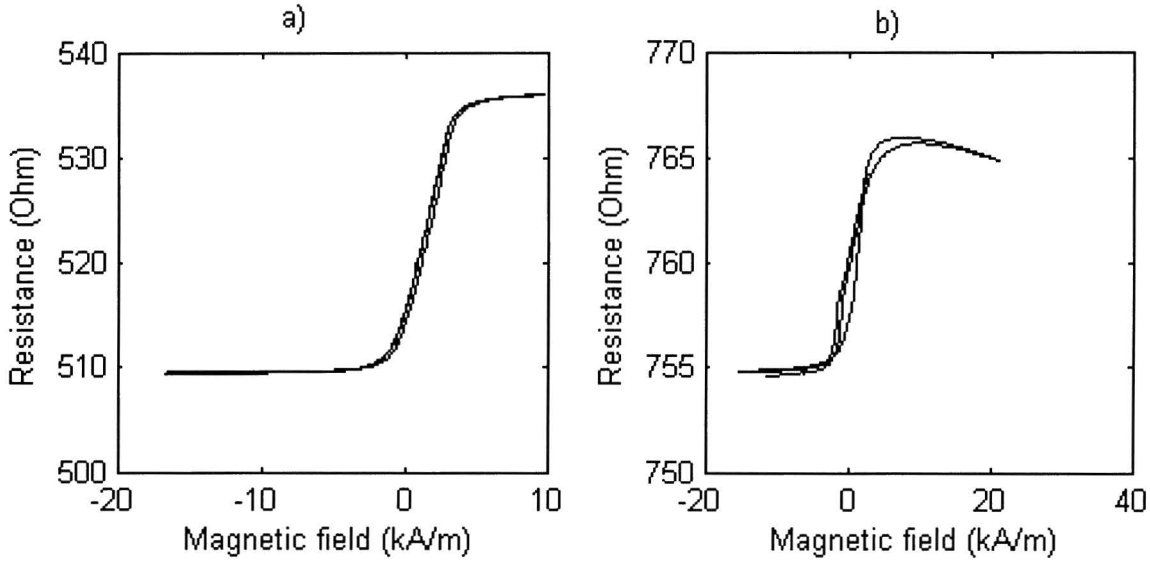

Figure 3.4: Magnetic field versus Resistance of GMR-stripe a) before change of resistance b) after change in resistance.

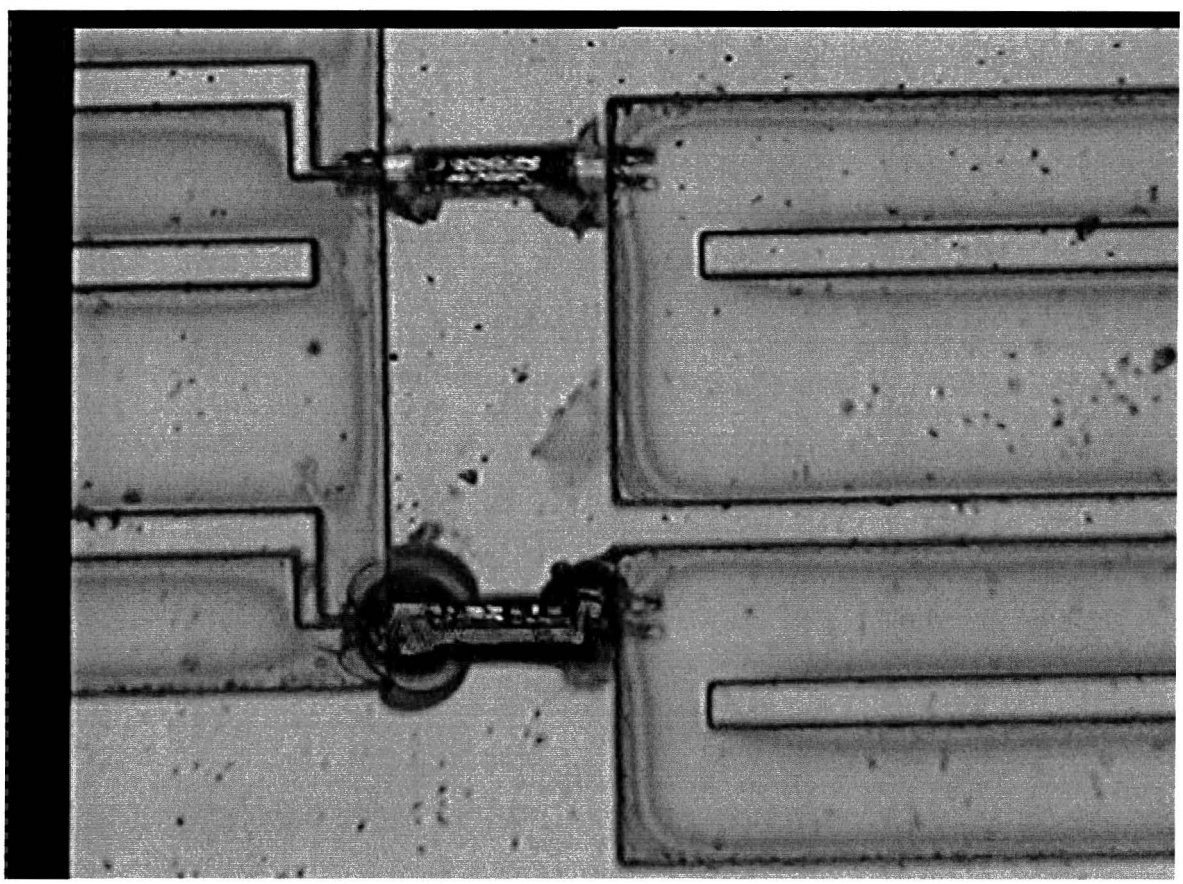

Figure 3.5: Picture of damaged Wheatstone bridge.

3.1.3. Flow cell

The biochip is glued on a printed circuit board (PCB). A flow cell is installed on the biochip for injection of magnetic nanobeads (Figure 3.6). The volume of the flow cell should be smaller than 8 µl, so that the amount of beads in the bulk solution is small. In the centre it has to be thin so the electromagnets can approach as close as possible. The height of the channel equals the height of the polydimethylsiloxane (=PDMS) seal (400 µm). This PDMS layer is then laid on the chip and on top of it is a quartz glass cover. The needle will inject the magnetic nanobeads. In a later state of the project a high pressure liquid cromatography pump will replace the needle. A small metal plate, which functions like a spring is holding the flow cell tight on the PDMS layer.

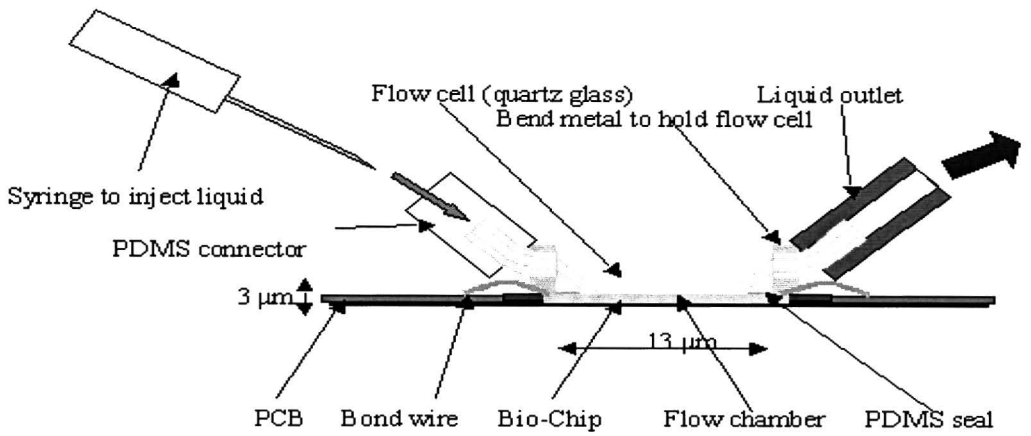

Figure 3.6: Sketch of the flow cell on the biochip.

3.1.4. Experimental set-up

We have a holder where we can place our sensor in (Figure 3.7). Because a misalignment of the external field of 0.8 kA/m in-plane component give a shift of 0.5 Ω in the GMR. This shift in the GMR can causes the GMR-stripe to saturate as the misalignment of the external magnetic field is too high. Therefore we have made the holder so that we can align the magnet with the biochip.

The current that is used for the sensor is provided by 3 times 1.5 V AA batteries with one series bulk resistance of 1 kΩ and a potentiometer with range 0 to 10 kΩ. The voltage over the 1kΩ resistance is recorded by a Keithley 2000 multimeter to regulate the current.

The sensor voltage V_s is measured by a Keithley 2182 Nanovoltmeter. We use this nanovolt meter because it has a resolution of 1 nV and has a noise level of 70 nV with a integration time of 20 ms and a dead time of 40 ms.

The coils of the magnet are driven by a coil driver, which by itself is driven by a function generator. The coil driver has 3 modes: the positive mode, the negative mode and the

bipolar mode (Figure 3.9). The amplitude that is used in our experiments will give us an external field of 8 kA/m Gauss.

All the devices are controlled by an computer which uses a Labview program.

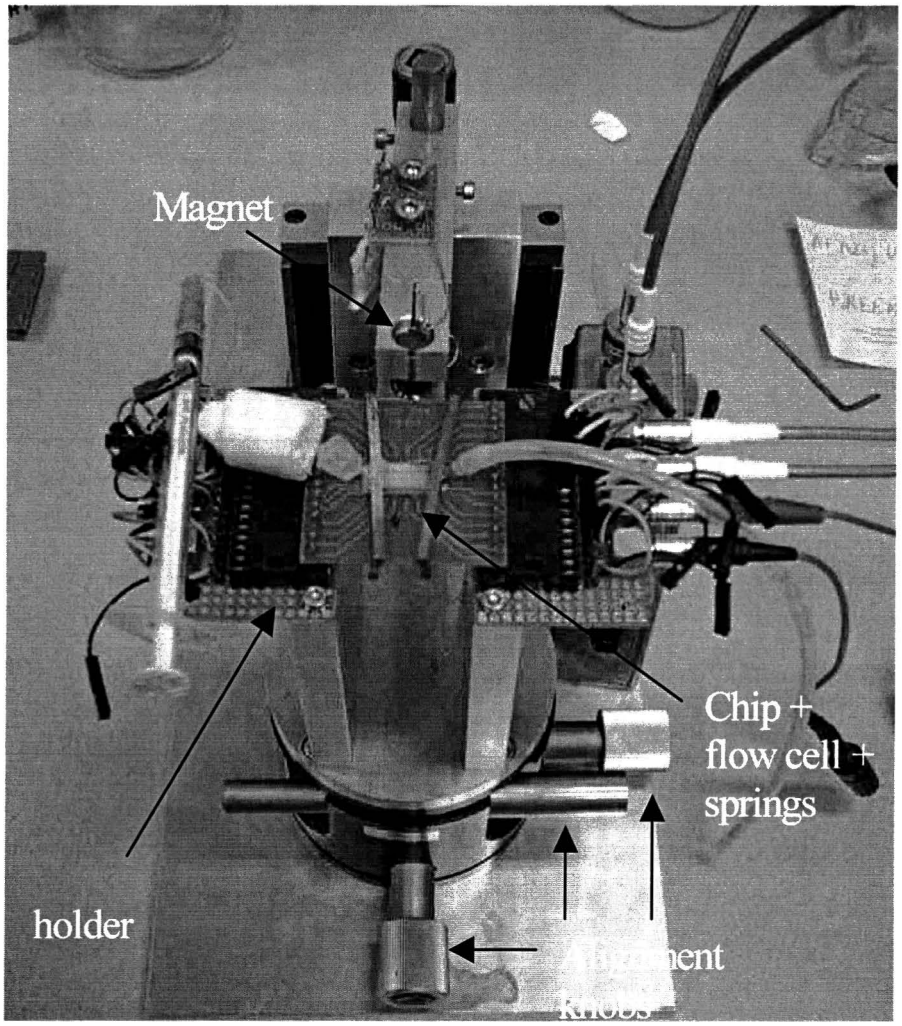

Figure 3.7: Sample holder and magnet.

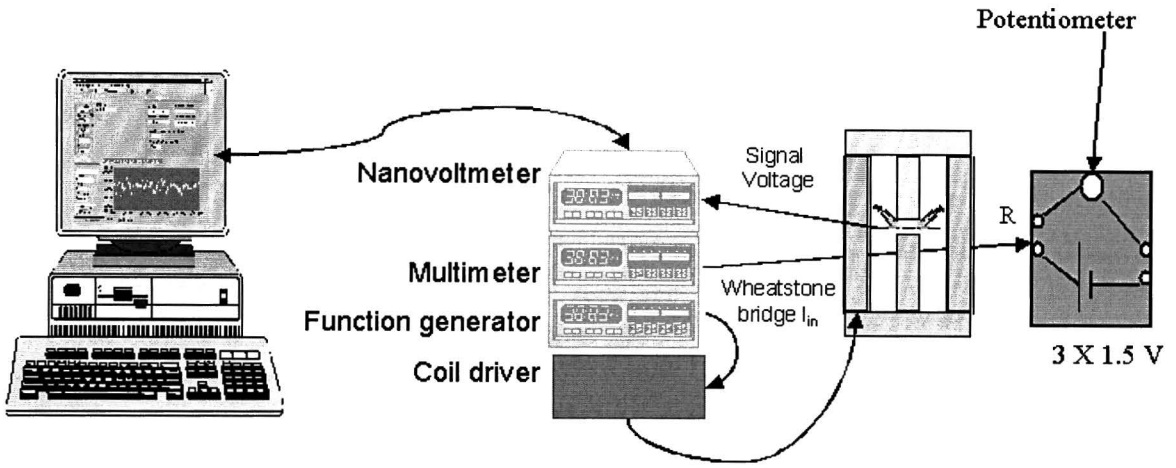

Figure 3.8: Experimental set-up of the beads experiment.

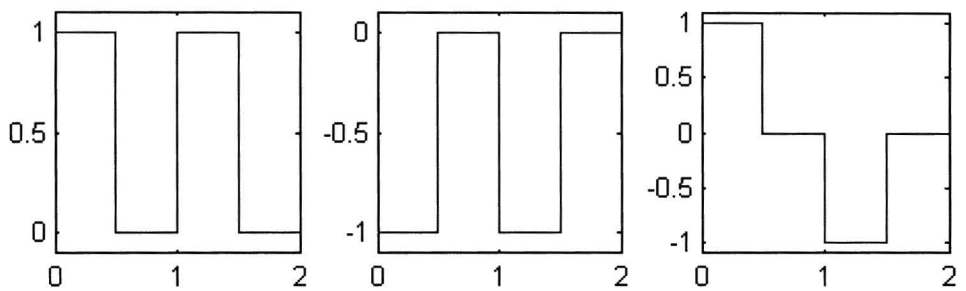

Figure 3.9: The 3 possible modes of the coil driver a) positive mode, b) negative mode, c) bipolar mode.

4. Results and discussion

4.1. Alignment of chip

When trying to align the sensor with the external magnetic field we saw that the GMR resistance also changed with the magnetic field (Figure 4.1). We saw that the GMR resistance sometimes did not follow the pulses of the magnetic field (Figure 4.1.a) and sometimes follow the pulses (Figure 4.1.b). The four GMR-stripes in the Wheatstone bridge are not perfectly matched, so we will see this unwanted effect in the Wheatstone voltage.

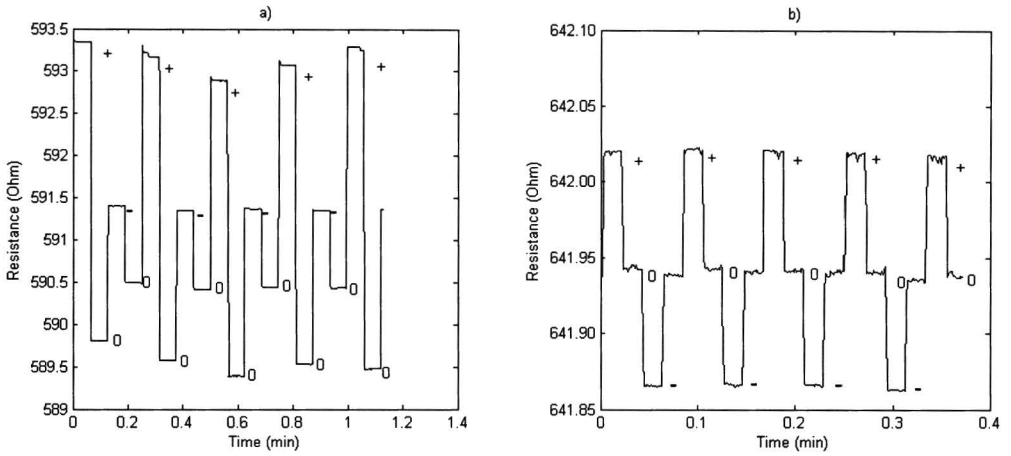

Figure 4.1: Difference in resistance response a) external magnetic field mostly in y-direction b) external magnetic field mostly in x-direction.

If the magnetic field is completely in the x-direction, perpendicular to the GMR-stripe and in-plane with the GMR stripe, we say that the angle is 0 degrees, if the magnetic field is completely in the y-direction, in the direction of the GMR-stripe, we say that the angle is 90 degrees (Figure 4.2). To understand the behaviour of Figure 4.1. we investigated the GMR resistance in function of different angles of magnetic field.

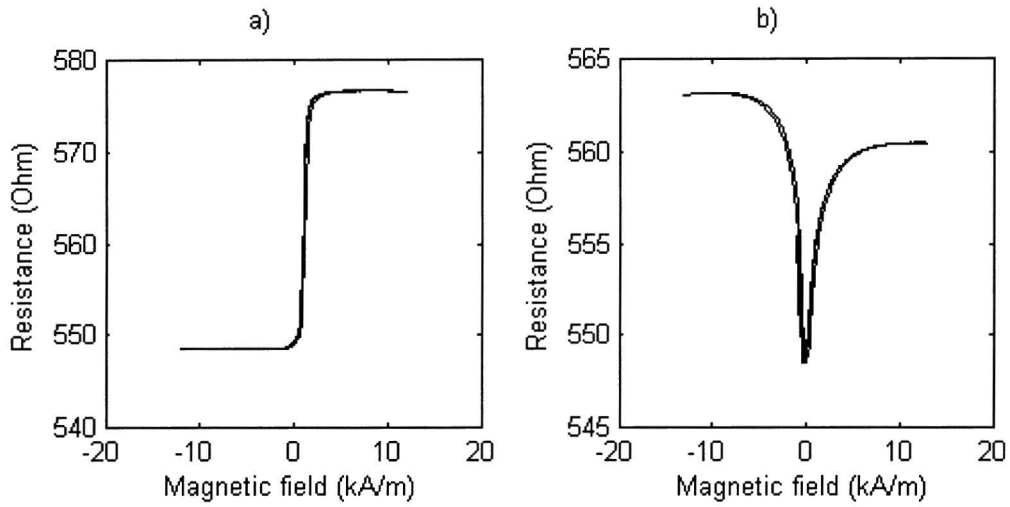

Figure 4.2: Resistance versus magnetic field, a) in-plane magnetic field perpendicular to the GMR and b) in-plane magnetic field along the GMR.

Figure 4.2.a shows the characteristics of the GMR-stripe we desire. The V-shape form of Figure 4.2.b is not useful for our application because the effect will cancel out in a perfect Wheatstone bridge. The reason that Figure 4.2.b is not completely symmetric is that the pinned layer has a little angle in the y-direction.. In Figure 4.3 you can see how resistance versus magnetic field for different angles (Appendix B). The GMR ratio is also dependent on the angle of magnetisation (Figure 4.4). You can see in Figure 4.4 that the MR_{ratio} is decreasing when the magnetic field changes more in the y-component.

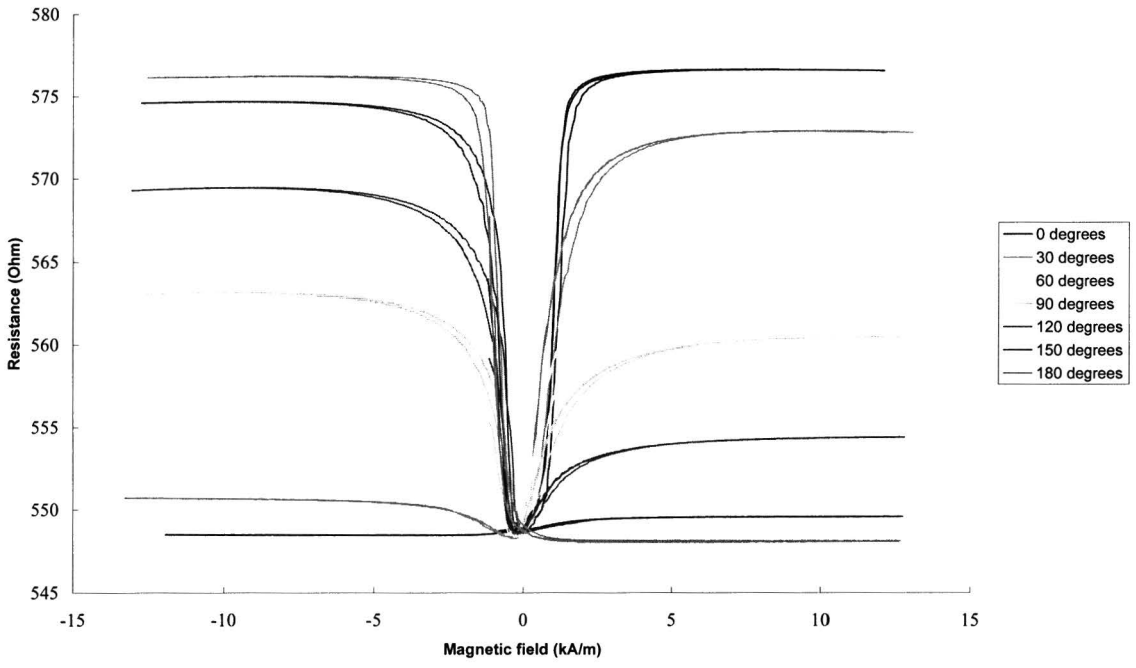

Figure 4.3: Resistance versus magnetic field for different angles.

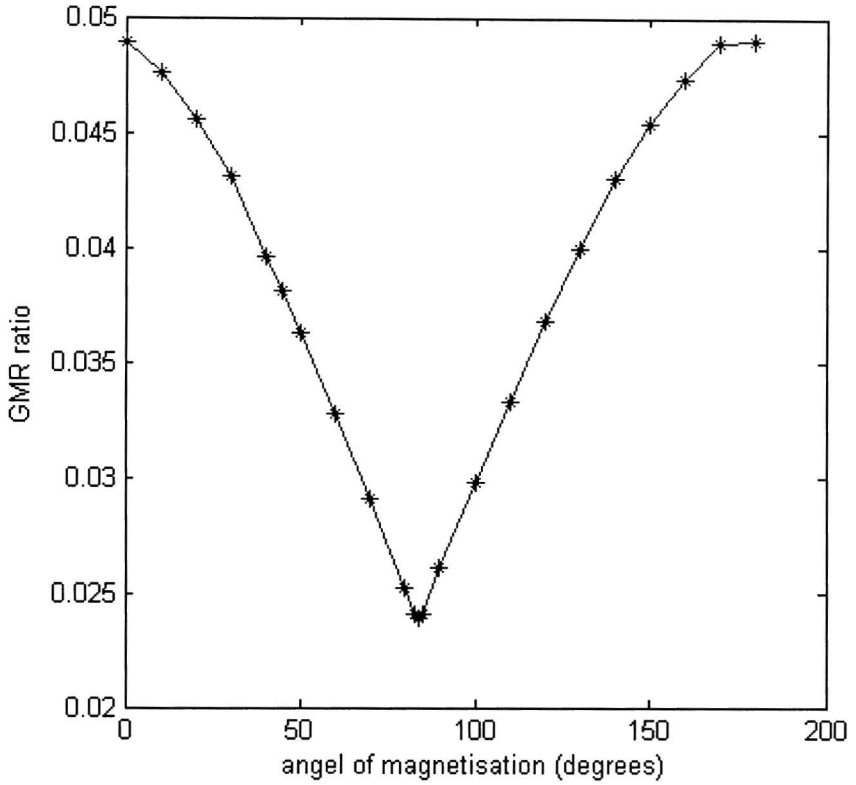

Figure 4.4: GMR_{ratio} versus angle of magnetisation

Figure 4.1.b can be explained that the external magnetic field has a misalignment in the x-direction while Figure 4.1.a can be explained that the external magnetic field has a misalignment in the y-direction while.

In the experiments we try to have to best possible alignment of the external field. This means that the Wheatstone voltage is insensitive to the external magnetic field and we are still in sensitive area of the GMR.

4.2. List of bead experiments

In this paragraph we will discuss results of the experiments performed. In each experiment we used a current *I* of 1mA and an external magnetic field of 8 kA/m. Before each experiment the external magnetic field was aligned with the chip in the optimal way. There were twelve different experiments performed which can be categorised into three groups, depending on the pre-treatment. In the first group the gold surface was pre-treated with Bovine Serum Albumin (BSA), a protein to prevent sticking, in the second group the surface was pre-treated with deionised millipore water and the in third with Biotinylated BSA, an protein to improve sticking. After the beads are injected, they are at rest. So there is no current in the flow cell. In Table 4.1 you can find a list of the experiments including the names used to refer to them later in the report.

Name	Date of experiment	Beads	Concentration (g/l)	Preparation procedure
Exp 1	29-10-2002	130 nm	0.2	BSA
Exp 2	29-10-2002	130 nm	1	Exp 1
Exp 3	02-12-2002	50 nm	0.1	Water
Exp 4	02-12-2002	50 nm	1	Exp 3
Exp 5	02-12-2002	130 nm	0.1	Exp 3-4
Exp 6	02-12-2002	130 nm	0.2	Exp 3-5
Exp 7	02-12-2002	130 nm	1	Exp 3-6
Exp 8	02-12-2002	50 nm	0.2	Biotinylated BSA
Exp 9	02-12-2002	50 nm	1	Exp 8
Exp 10	02-12-2002	130 nm	0.1	Exp 8-9
Exp 11	02-12-2002	130 nm	0.2	Exp 8-10
Exp 12	02-12-2002	130 nm	1	Exp 8-11

Table 4.1: Schedule of bead experiments

To elaborate, in Exp 2 the beads (concentration 1g/l) were added following completion of Exp 1, hence Exp1 is detailed as the preparation step for Exp 2. The data of the experiments are given in Appendix A.

4.3. Experiments with beads

In this paragraph the experiment will be described. The signal processing will be explained through Exp 1 (Figure 4.5), where the output voltage is the measured voltage across the Wheatstone bridge.

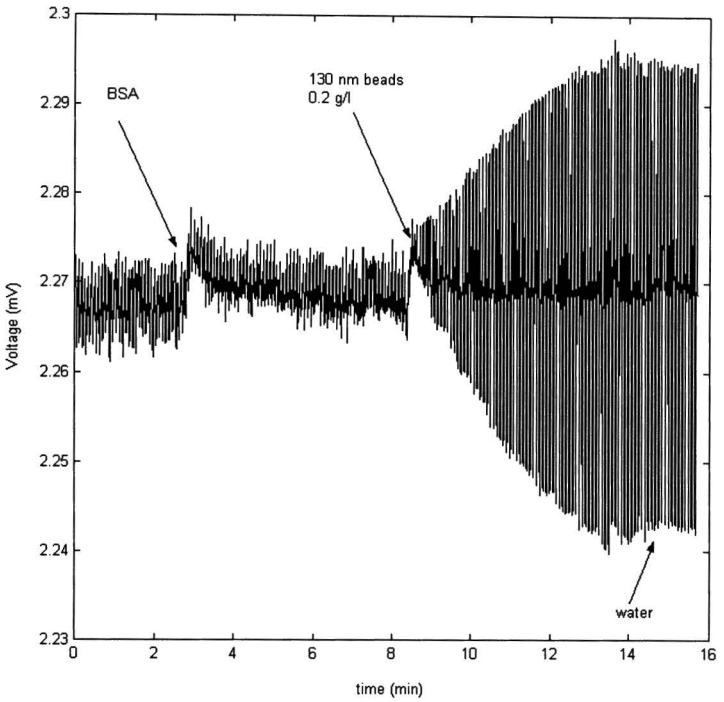

Figure 4.5: Weatstone bridge voltage versus time of expermiment 1, with a period of field switch of 4.986 s.

At 2'40'' BSA was injected, then at 8'24'' 130 nm beads with a concentration of 0.2 g/l wer injected, and finally at 14'06'' water was injected to flush the beads away. In all the experiments the beads were washed away by rinsing with pure water, except in Exp 1 and 2. After Exp 2 we tried to wash the beads away by injecting a phosphate buffer saline (PBS) which has a 0.1 M [PO_4^{3-}] and 0.15 M [Cl^-]. Afterwards a HCl solution of 0.05 M was injected and a KCl solution of 0.05 M. These solutions did not wash the beads off.

The Wheatstone voltage before injection of magnetic beads is not zero. This is due to the fact that not all the GMR resistances are all the same, so the bridge is not fully balanced. During experiments we use a bipolar magnetic pulse, with a cycle time of 4.986 seconds. At t = 0 the positive pulse begins, so at t = 4.986 the second positive pulse starts. Each 60 ms we have a data point. The voltage we measure in the Wheatstone bridge, before the injection of the beads, follows the pulses of the external magnetic field. This extra voltage is due to the misalignment of the magnet as explained in § 4.1 (Figure 4.1).

We average output voltage for the interval between 10 % and 90 % of the positive pulse length in order to exclude errors such as the switching transient. We also average for both the voltage at zero magnetic fields and the voltage at negative magnetic field (Figure 4.6 and Figure 4.7).

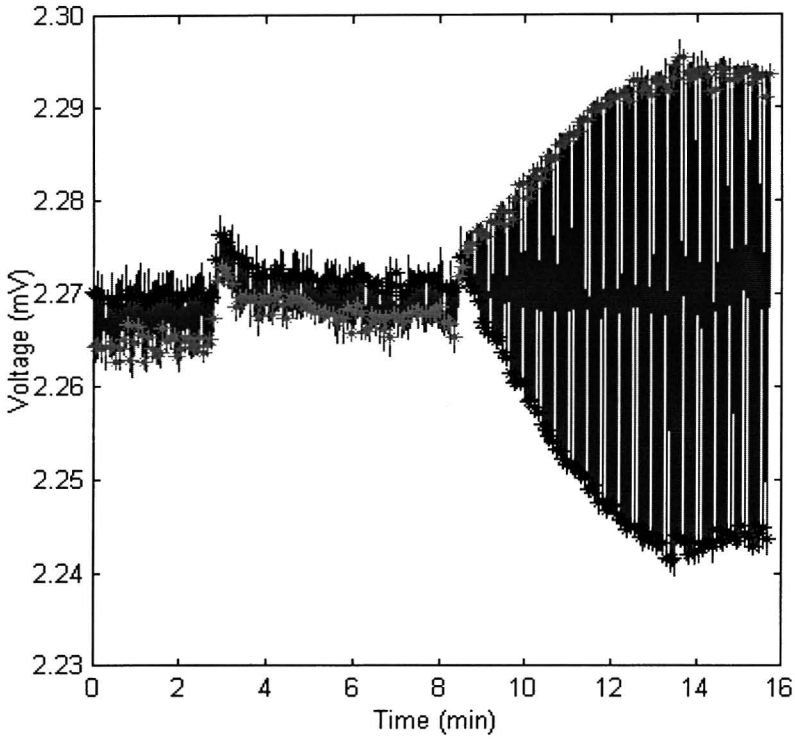

Figure 4.6: Wheatstone bridge voltage of Exp 1 versus time (blue), average of the voltage at the positive pulse (black), average of the voltage at the negative pulse (red).

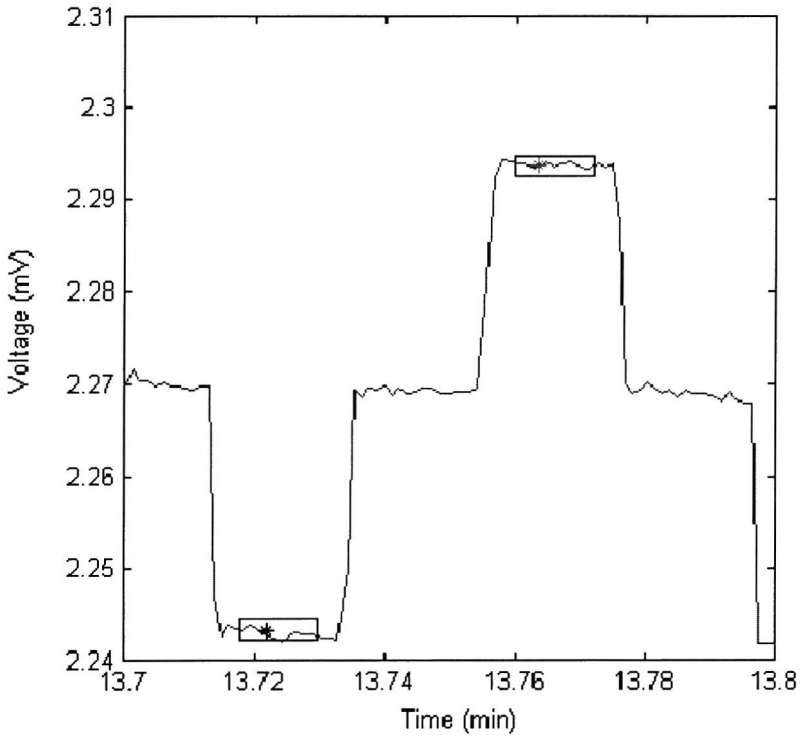

Figure 4.7: Wheatstone bridge voltage of Exp 1 versus time for the time interval [13,7-13,8]

In Figure 4.6 and Figure 4.7 the Wheatstone bridge voltage versus time is plotted in blue, also the averaging of the voltage at positive pulses, $\overline{V_+}(n)$, is plotted in black, and the averaging of the voltage at negative pulses ,$\overline{V_-}(n)$, is plotted in red. To derive the $V_s(n)$ we subtract the voltage of the positive pulse from the voltage of the negative pulse:

$$V_s(n) = \frac{\overline{V}_+(n) - \overline{V}_-(n)}{2} \qquad (4.1)$$

were $\overline{V_+}(n)$ is the average value of the nth positive pulse, and $\overline{V_-}(n)$ is the average value of the nth negative pulse. The signal voltage, $V_s(n)$, of experiment 1 can be seen in Figure 4.8.

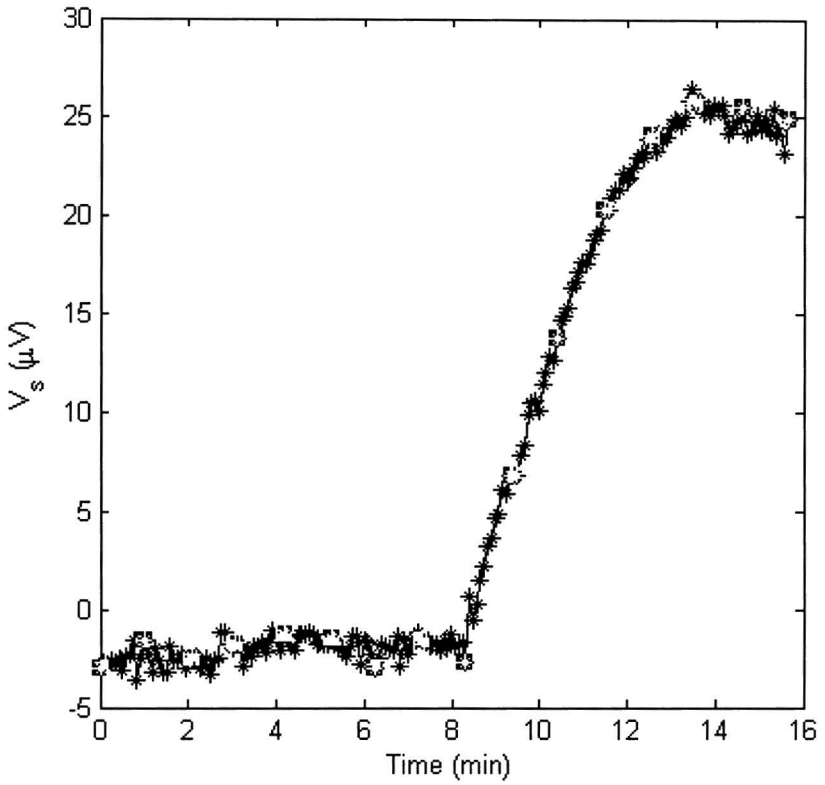

Figure 4.8: Signal voltage, V_s, *(4.1) versus time of Exp 1.*

By using (2.18), and (2.24), the *maximum voltage* equals 27.9 ± 0.2 μV, this is the signal voltage, V_s, when it saturates minus the signal voltage before injection. When the signal voltage, V_s, saturates, we suppose that the beads are in an homogenous concentration in the channel. The signal voltage, V_s, before injection is due to the misalignment of the external magnetic field. The injection of the BSA did not give an increase in signal voltage, V_s. In some experiments the signal voltage, V_s is noisier than in others. This will be explained in §4.4. Results of further experiments are given in Appendix A.

The signal voltage, V_s, has a bulk part and a surface part. By using (2.13) I = 1 mA, s_{GMR} = 5 10^{-3} Ωm/A, and the dimensions of §2.3.2, we can rewrite the signal voltage, (2.15), that results from the bulk contribution as:

$$V_s = 2.24 \cdot 10^{-6}\ mN \qquad (4.2)$$

We see that (4.2) depends on the magnetic moment of the beads and the concentration of beads in solution (*mN*). Since the unit of *mN* is A/m, we can call this the fluid magnetisation. In Table 4.3 the name of the experiment, the fluid magnetisation as deduced from the magnetisation per gram of beads ((2.25) and (2.41)) and the concentration (Table 4.1), the maximum signal voltage, V_s, and the preparation procedure are given for each experiment.

Name	Beads	C (g/l)	N*m (A/m)	Maximum signal (μV)	Theoretical bulk signal (μV)	Beads per μm^2
Exp 1	130 nm	0.2	7.14 ± 0.7	27.9 ± 0.2	16.0	0.17
Exp 2	130 nm	1	35.7 ± 3.6	30.7 ± 0.3	80.0	-0.69
Exp 3	50 nm	0.1	0.91 ± 0.1	1.5 ± 0.1	2.0	-0.60
Exp 4	50 nm	1	9.1 ± 1.0	9.0 ± 0.2	20.3	-12.6
Exp 5	130 nm	0.1	3.6 ± 0.4	36.7 ± 1.3	8.11	0.40
Exp 6	130 nm	0.2	7.1 ± 7.1	42.0 ± 3.1	15.9	0.36
Exp 7	130 nm	1	35.7 ± 3.6	78.2 ± 11.4	80.0	-0.02
Exp 8	50 nm	0.2	1.81 ± 0.2	2.2 ± 0.1	4.05	-2.06
Exp 9	50 nm	1	9.1 ± 1.0	5.2 ± 0.1	20.3	-16.9
Exp 10	130 nm	0.1	3.57 ± 0.4	46.9± 1.5	8.0	0.53
Exp 11	130 nm	0.2	6.92 ± 0.7	70.1 ± 2.6	16.0	0.75
Exp 12	130 nm	1	35.7 ± 3.6	65.1 ± 2.1	80.0	-0.21

Table 4.2: Table of experiments with maximum signal, theoretical bulk signal and theoretical beads per μm^2 (Table 4.1).

In Figure 4.9 we give the *maximum signal* versus the fluid magnetisation. The straight line in the figure is the theoretical bulk voltage calculated from (4.2). The actual result of each experiment that was conducted, is the sum of a bulk part and a surface part. The bulk part is bulk concentration-determined, whereas the surface part is surface-concentration determined. The surface part is due to unspecific bounding of the beads with the surface. The signal voltage, V_s, increases with concentrations of beads. If we subtract the theoretical bulk voltage from the signal voltage, V_s, and divide this by the theoretical surface voltage of 1 bead per μm^2, we can estimate the number of beads per μm^2 (Table 4.1). From Table 4.2 it can be observed that the experiments with the 130 nm beads have the same order of beads on the surface except in Exp 2. The experiments with the 50 nm beads have a lower signal voltage, V_s, compared at the same fluid mag-

netisation as the 130 nm beads. A possible explanation of the lower signal voltage, V_s, of the 50 nm beads is that the 50 nm beads don't stick to the surface as good as the 130 nm beads, because of the lower surface contact. The fact that the voltage signal is not as high as we expected can have four reasons: (i) a lower external magnetic field during the experiment, causing a lower fluid magnetization, (ii) clustering of beads, giving a lower fluid magnetization than expected, and (iii) misalignment of the channel with respect to the GMR stripes (iv) the volume concentration above the sensor is not the same as the bulk volume concentration that we injected. Optical images showed that experiments 3 to 12 were performed with a Wheatstone bridge having a misalignment of the channel of 1.2 μm. This channel misalignment will decrease the signal (2.11) by 23 % for the surface method and 18 % for the bulk method.

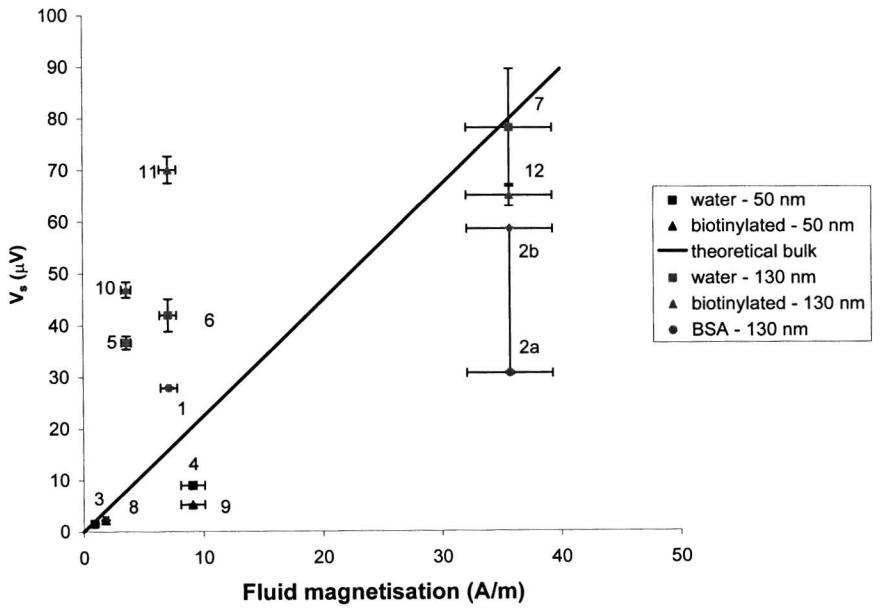

Figure 4.9: Signal voltage, V_s, versus fluid magnetisation.

In Figure 4.9 Exp 2 has two points, 2a and 2b. This is because during all the experiments we could wash off the beads so that the signal was the same after injection as before injection of the beads except after experiment 1 and 2 (*Figure 4.10*). The point 2a is the maximum signal is calculated from saturation signal minus the signal before injection and 2b is calculated from the saturation signal minus the signal of the beginning of the experiment.

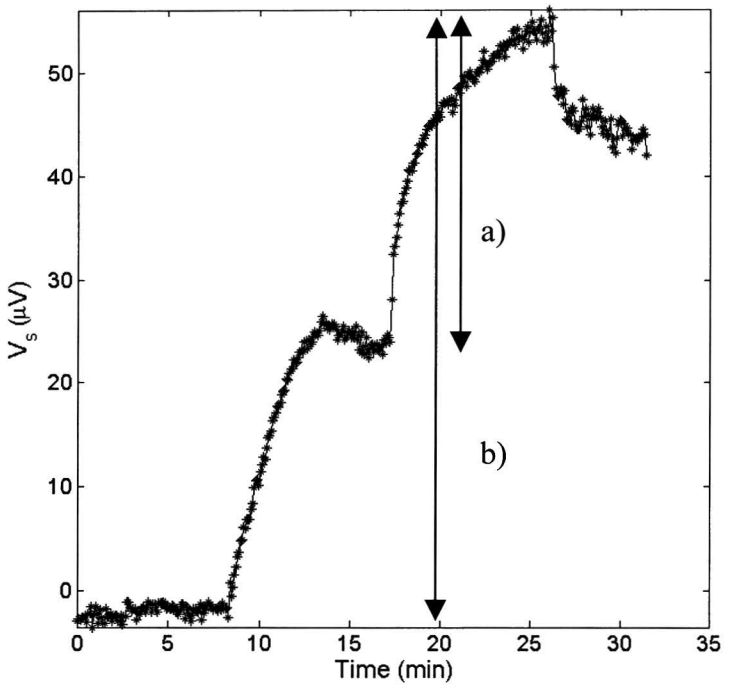

Figure 4.10: Voltage signal of Exp 1 + 2.

4.4. Remanance

In Exp 5-6-7-10-11-12 we observe strong fluctuations of the signal voltage, V_s (Figure 4.11).

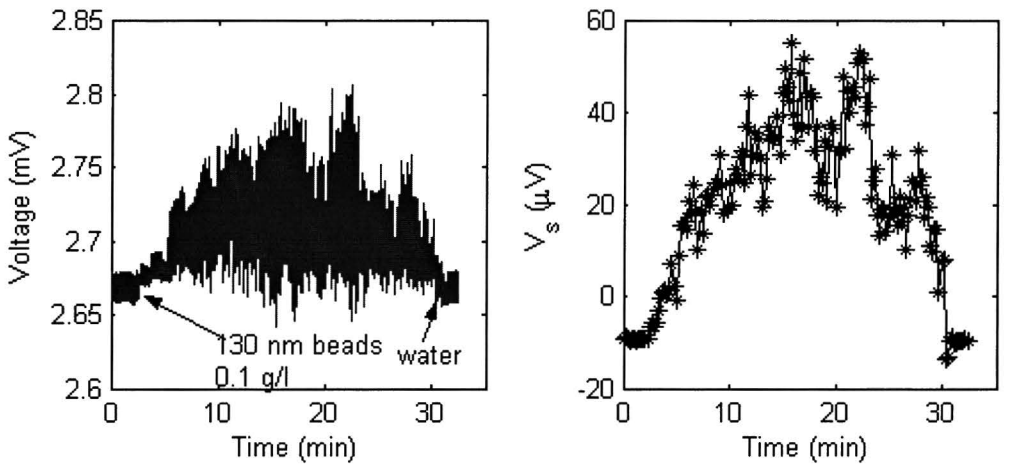

Figure 4.11: Voltage versus time and signal voltage versus time of experiment 5.

In addition to the fluctuation, we observed a remanence of the beads. For that reason we calculate the *Remanence(n)*:

$$V_R(n) = \overline{V}_O(2n-1) - \overline{V}_O(2n) \qquad (4.3)$$

were $V_O(n)$ is the average voltage at the nth zero-held interval. For each period the $V_R(t)$ is the difference between the voltage at the zero field after the positive pulse is applied and

the zero field after the negative pulse is applied. The time dependence of $V_R(n)$ for Exp 1 and at 5 can be seen in (Figure 4.12).

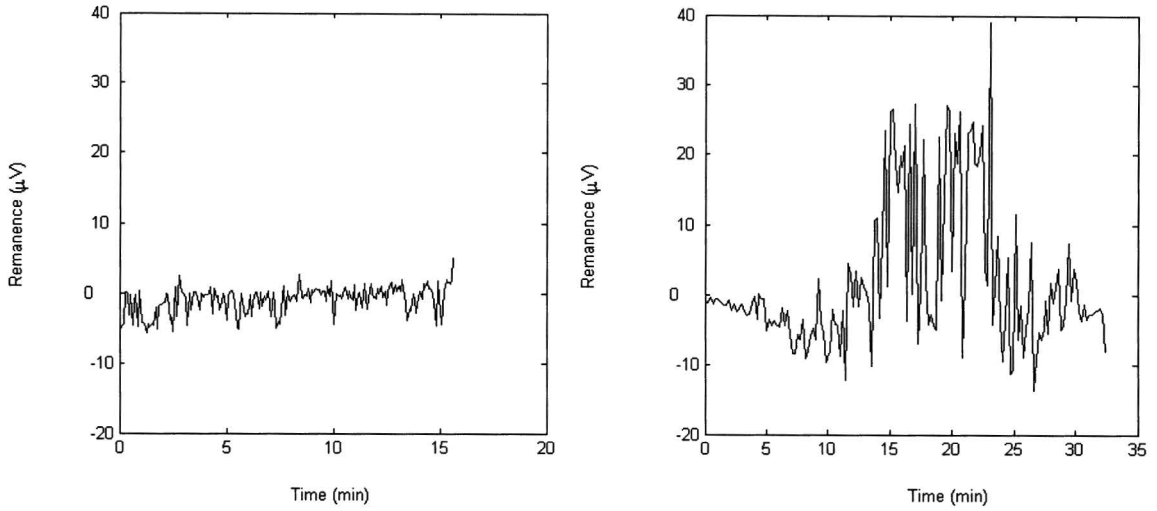

Figure 4.12: Remanence versus time of Exp 1 on the left and Exp 5 on the right.

The beads used in Exp1 and Exp 5 were both the 130 nm with a concentration of 0.1 g/l. We see that the *Remanence* of Exp 1 is a lot lower than the *Remanence* of Exp 5. A possible reason to explain this is that the beads formed clusters and are not superparamagnetic anymore. A way to improve this, is to filter the beads before injection.

4.5. Slopes correlated to diffusion

The signal voltage, V_s, of the experiments does not jump to its saturation value immediately. This is because the beads have to diffuse towards the sensor. Therefore we plot the square root of t-t_0, versus signal voltage, V_s, (Figure 4.13). The slope of the line is 14.7 $\mu V/min^{1/2}$. This value is an indication for the diffusion speed. The slope is a measure for the diffusion constant. More elaborate analysis has not been performed.

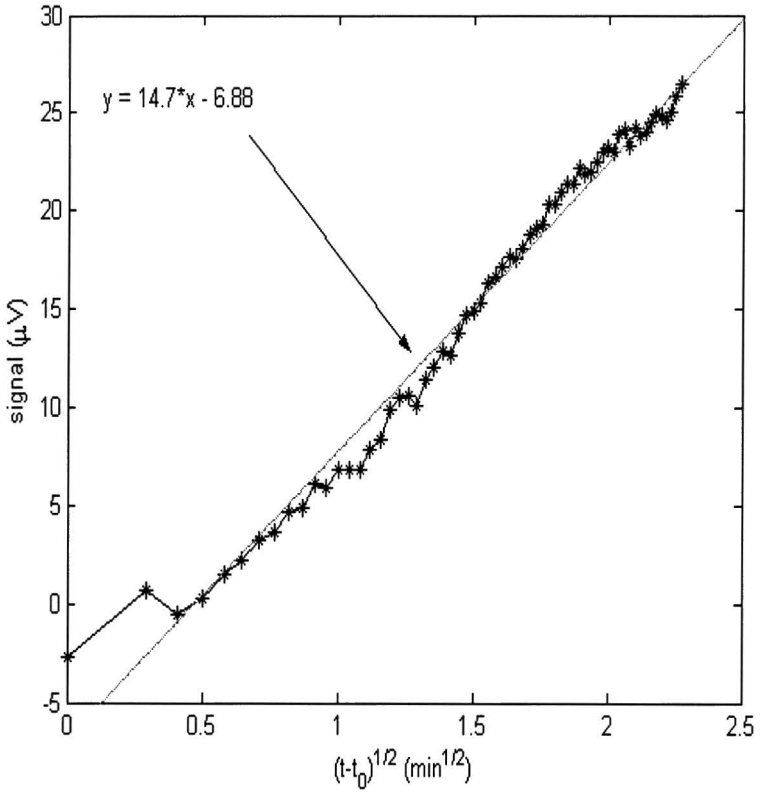

Figure 4.13: Signal voltage, V_s*, versus the square root of time relative to injection of beads.*

In Table 4.3 the name of the experiment, the fluid magnetisation, the slope $\frac{dV}{d\sqrt{t-t_0}}$ and the preparation procedure are given for each experiment.

Name	N*m	Slope $\left(\mu V/\sqrt{\text{min}}\right)$	Preparation procedure
Exp 1	7.14 ± 0.7	14.7	BSA
Exp 2	35.7 ± 3.6	10.9	Exp 1
Exp 3	0.91 ± 0.1	0.31	Water
Exp 4	9.1 ± 1.0	1.4	Exp 3
Exp 5	3.6 ± 0.4	16.4	Exp 4
Exp 6	7.1 ± 7.1	15.8	Exp 5
Exp 7	35.7 ± 3.6	73.7	Exp 6
Exp 8	1.81 ± 0.2	0.73	Biotinylated BSA
Exp 9	9.1 ± 1.0	4.4	Exp 8
Exp 10	3.57 ± 0.4	16.2	Exp 9
Exp 11	6.92 ± 0.7	21.2	Exp 10
Exp 12	35.7 ± 3.6	79.3	Exp 11

Table 4.3: Table of experiments with slope.

From Table 4.3 we can plot the slope $\frac{dV}{d\sqrt{t-t_0}}$ versus the cumulative magnetic moment (Figure 4.14). From Figure 4.14 it can be observed that the slope $\frac{dV}{d\sqrt{t-t_0}}$ for each fluid magnetisation is comparable, independent of preparation procedure of the surface, except experiment 2. We suspect a linear relationship between the slopes $\frac{dV}{d\sqrt{t-t_0}}$, but to ascertain this further experimentation is required. The slopes increases with concentration as expected.

As shown in Figure 4.8 the diffusion time (time that the signal reach the saturation level) is around 5 minutes. The distance that a bead of 100 nm diffuses in 5 min is around 36 μm, while the height of the channel is only 3 μm. This means that the diffusion we measuring is not the diffusion solely into the channel.

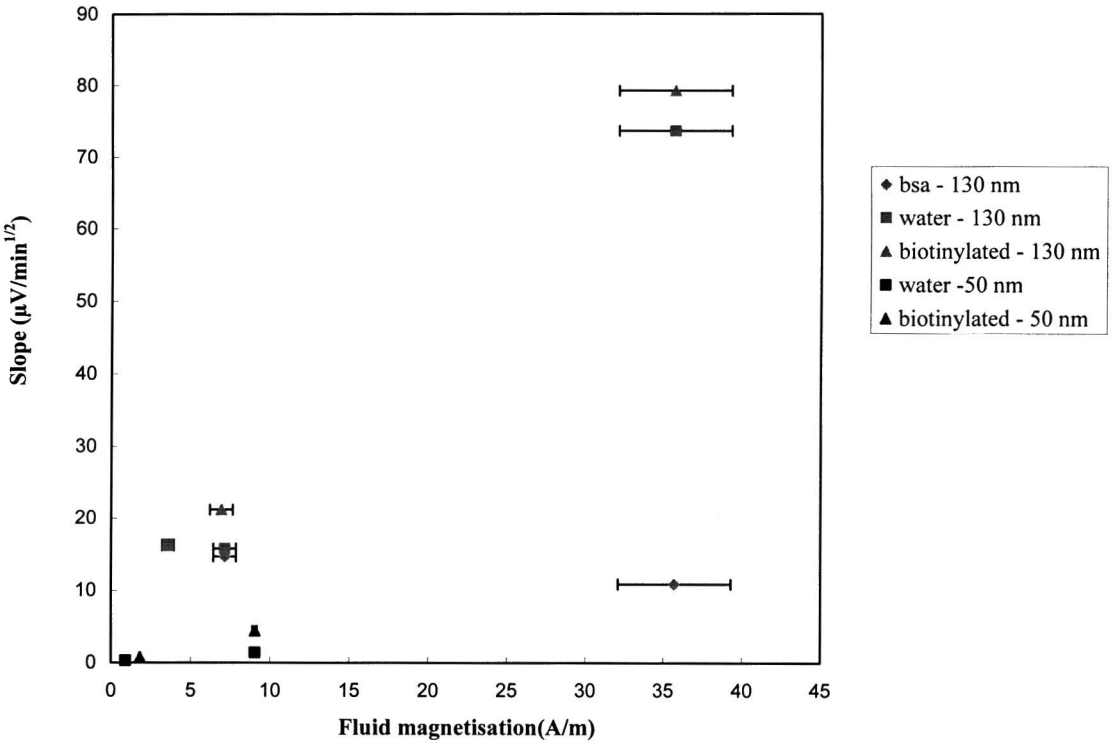

Figure 4.14: The slope $\frac{dV}{d\sqrt{t-t_0}}$ *versus fluid magnetisation.*

5. Conclusions and recommendations

The purpose of this traineeship was to experimentally prove the detection of superparamagnetic nanobeads using a GMR device. We demonstrated experimentally (Figure 4.8 and Figure 4.9) that we can detect superparamagnetic nanobeads. The measured voltage is due to both bulk and surface contributions. The surface component is larger for the 130 nm beads than for the 50 nm beads, due to stronger adhesion of the 130 nm beads. It is also shown that the signal voltage, V_s, increases with concentration. The *Slope*, which is an indication of how fast the signal voltage, V_s, goes to saturation, increases with concentration.

We demonstrated experimentally that the beads can have remanence. We suppose that this is due to clustering. It is advisable to filter the bead solution and characterise the beads by optical measurement methods.

We can estimate the low detection limit for nanoparticles by GMR. The Wheatstone bridge voltage (see equation (2.11) and (2.15)) is dependent of the chip layout and four other variables: the current I, the sensitivity of the GMR-stripes s_{GMR}, the magnetic moment of the beads m, and the concentration, n. From this concentration, n, we can calculate the concentration of target. To lower the detection limit and improve the sensitivity we have to alter the other variables. The s_{GMR} is dependent on the stack of materials that is used and the length of the stripe. This dependence is proportional with the length. The length that is used on the experiments is 100 μm and can be increased to 1000 μm on a real chip. In future it should be possible to make GMR-stripes of different stacks that are four times more sensitive [11]. To improve the magnetic moment of the beads, m, we have to bring the beads into saturation, with an external magnetic field of 80 kA/m. At that external magnetic field it is possible to find superparamagnetic nanobeads with a magnetic moment of 10^{-16} Am^2. Such beads have a diameter of about 100 nm. We need that a Wheatstone voltage of 1 μV to gives us a sufficient signal to noise ratio (SNR). The model with uniform magnetization (2.11) predicts a detectable surface density of $2 \cdot 10^{-4}$ beads per μm^2. This means that the surface where the beads will attach has to be at least 100 μm^2. It also means that our uniformity assumption is incorrect, and that we need to model the signal for discrete particles. Nevertheless. Let us continue with the calculated number. If we have 1000 antibodies per square μm, and K_{eq} of 10^{-12} l/mol we can measure in theory a concentration of $2 \cdot 10^{-19}$ mol/l (Appendix D). The detection of such low concentration may be complicated by diffusion and time limitations, but it should be possible to measure in the range of femtomolar within minutes. Calculations in Appendix D show that we could be able measure 2 10^{-4} beads per μm^2. An assumption in the theory is that we have a homogenous magnetization across the sensor which will not be the case for such low surface concentration. Calculations need to be made in this low concentration range. It will also be useful to simulate what happens if we change the dimensions of a chip. Another important parameter in our experiments is diffusion. It is important to bring the beads as fast as possible to the surface to minimize the measuring time.

During the traineeship we had only four chips available to do experiments. In the future it is recommended to have more chips available to do more experiments. Recommended experiments will be to use different bead concentrations, and different surface treatments, to get a better understanding of the relationship of signal voltage, V_s, versus concentration, and *Slope* versus concentration. To get a better understanding of the noise and to know at which frequencies we have to modulate the external magnetic field, noise experiments have to be conducted. Important steps for the future are to use beads with higher magnetic moment, to make new chips with microfluidic package for a higher number of devices, and to prove the detection limit for biological targets.

6. Technology assessment

Early detection is very important in biological and bio-medical applications. Important examples are oncology, infections disease, food diagnostics, etc. Early detection requires very sensitive measurements of a wide range of bio-molecules, for example proteins and nucleic acids. To measure low concentrations we are using a biosensor. A biosensor is an analytical device that integrates a biological element with a signal transducer. This example sketches a sandwich assay. The biological element, for example antibodies, is a layer of capture molecules for specific interaction with the target. Biochips measure many targets at the same time, this is called multiplexing or lab on a chip. The perfect biosensor should feature a low detection limit, high sensitivity, be quantitative and fast while maintaining a low production cost. Biosensor detection principles can be electrical, magnetic, optical, or mechanical. This depends on the label which is used. The standard detection principle is optical, and has a detection limit of between 0.1 and 1 fluorescent molecule per square micrometer.

Our goal is to outperform fluorescent detection by two orders of magnitude. This kind of detection limit is not possible with current technology. We try to develop a magnetic biosensor using Giant MagnetoResistance (GMR), which has a potential to detect $2\ 10^{-4}$ labels per μm^2. A GMR-stripe consist of layers of magnetically different material which give a resistance change response under magnetic fields. Biological materials are generally not magnetic so the background signal during operation is low.

References

[1] Wild, David, e.a., *The Immunoassay Handbook*, Nature publishing groep, ISBN 1-56159-270-6 (2001).

[2] Baumgartner, M., *A GMR Biosensor Using Superparamagnetic nanobeads,* internal report, Nat.Lab. Technical Note 2002/094, Philips Research Laboratories, Eindhoven Netherlands (2002).

[3] Baselt, D.R., et.al, *A biosensor based on magnetoresistance technology*, Biosensors and Bioelectronics 13, 731-739 (1998).

[4] Coehoorn, R., *Giant magnetorisistance in exchange-biases spin-valve layered structures and its applications in read heads*, chapter 4 of Magnetic multilayers and giant magnetoresistance: fundamentals and industrial applications, Springer Series in Surface Sciences, Vol 37, U.Hartmann (ed.), p.65-127, Berlin (2000).

[5] http://electron6.phys.utk.edu/phys594/Tools/e&m/summary/magnetostatics /magnetostatics.html

[6] Buckingham, M.J., *Noise in electronic devices and system*, Ellis Horwood Limited, ISBN 0-85312-218-0 (1983).

[7] Veerdonk v.d., R.J.M., *Spin polarized transport in magnetic layered structures*, Technische Universiteit Eindhoven, ISBN 90-386-0817-9 (1999).

[8] Squires, G.L., *Practical Physics*,McGraw-Hilll book Company, pp.1-56,(1976).

[9] Kampen v., M., *Tunnel junctions: Noise and Tunnelling*, Afstudeerverslag Technical University of Eindhoven (1998).

[10] Thilwind, R.E., *Manipulation of superparamagnetic nanobeads for bio-molecular diagnostics*, Nat.Lab. Technical Note 2002/484, Philips Research Laboratories, Eindhoven Netherlands (2002).

[11] www.electrochem.org/meetings/past/202/abstracts/abstracts/k2/0531.pdf

A Figures of experimental data

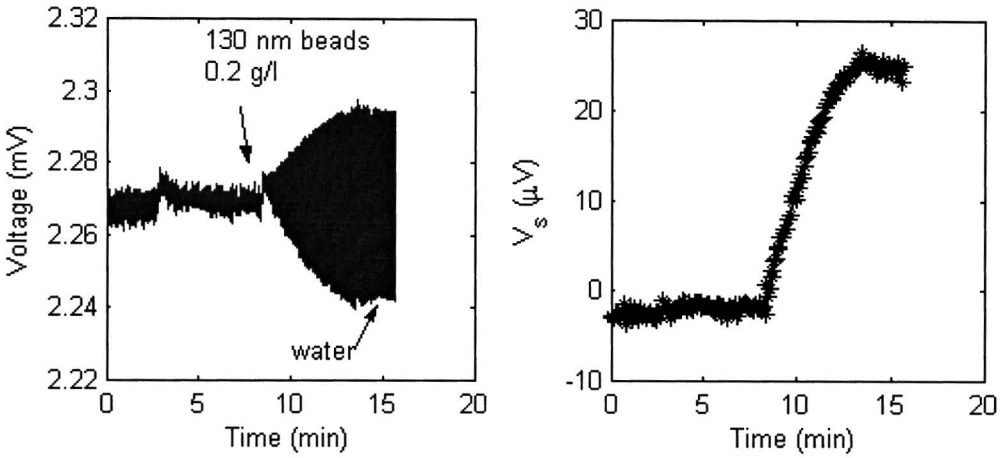

Figure A.1: Voltage versus time and signal voltage versus time of experiment 1.

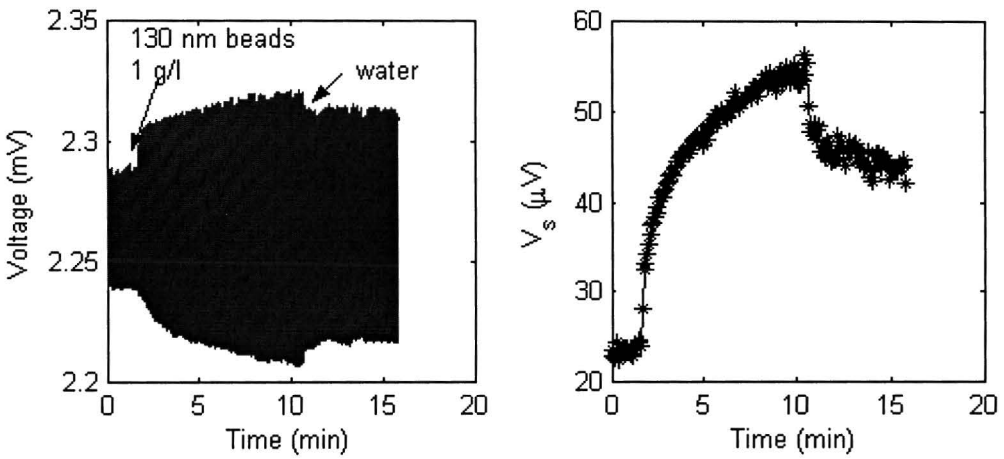

Figure A.2: Voltage versus time and signal voltage versus time of experiment 2.

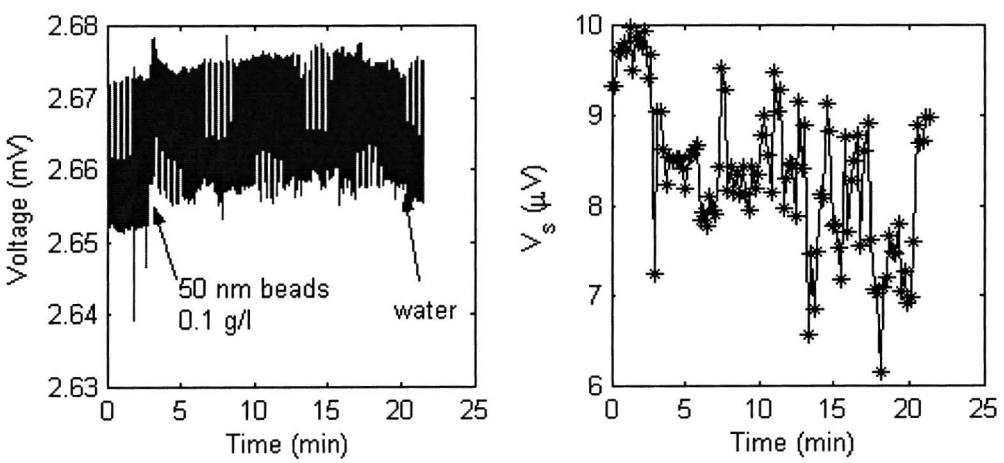

Figure A.3: Voltage versus time and signal voltage versus time of experiment 3.

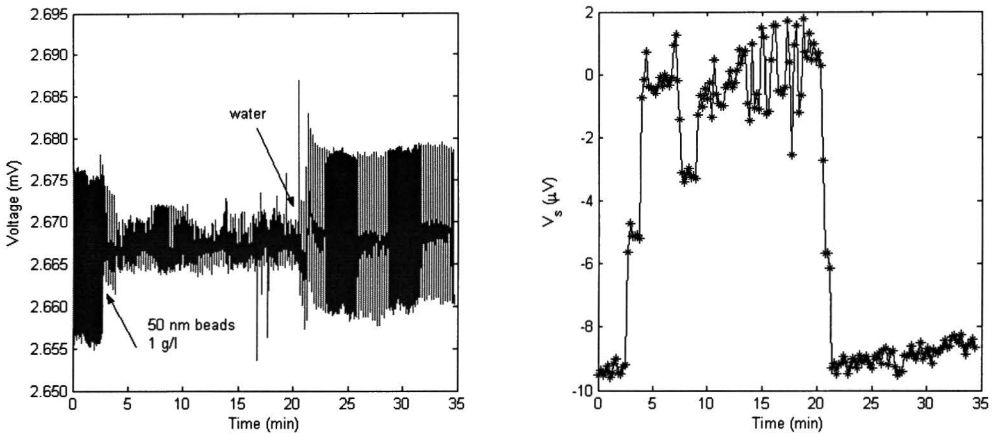

Figure A. 4: Voltage versus time and signal voltage versus time of experiment 4.

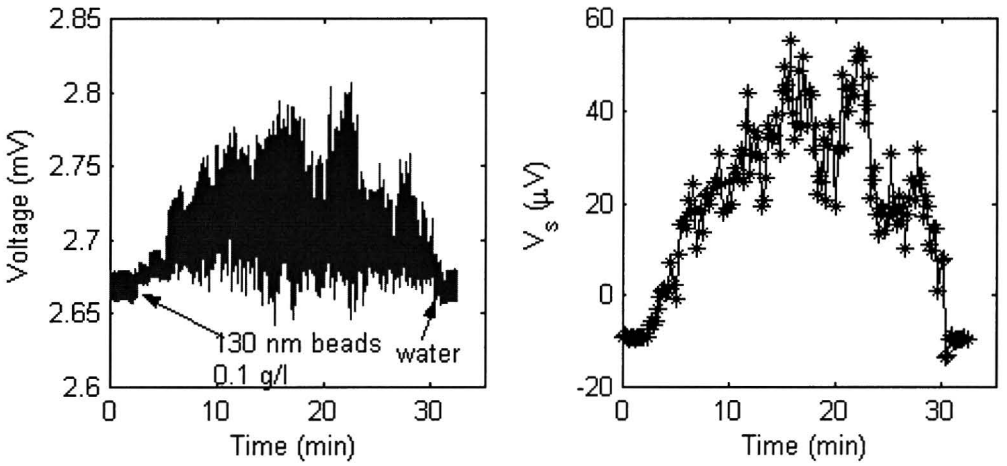

Figure A.5: Voltage versus time and signal voltage versus time of experiment 5.

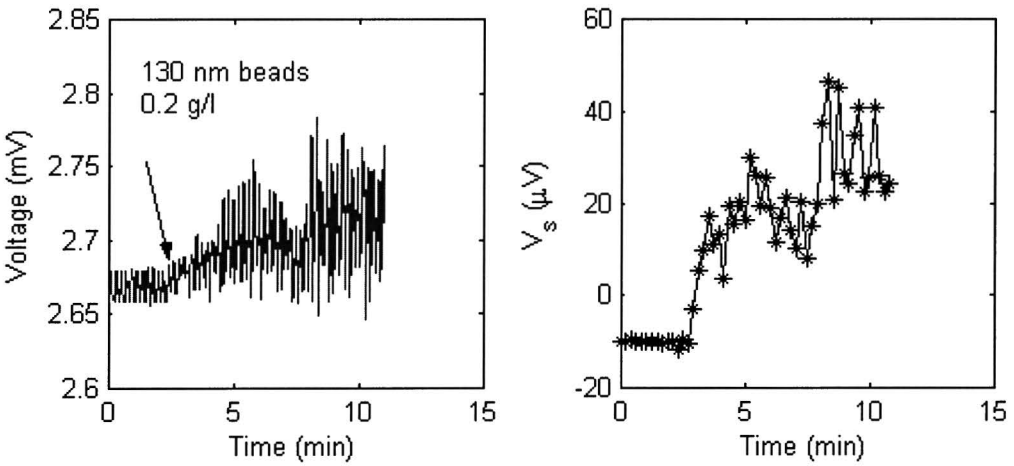

Figure A.6: Voltage versus time and signal voltage versus time of experiment 6.

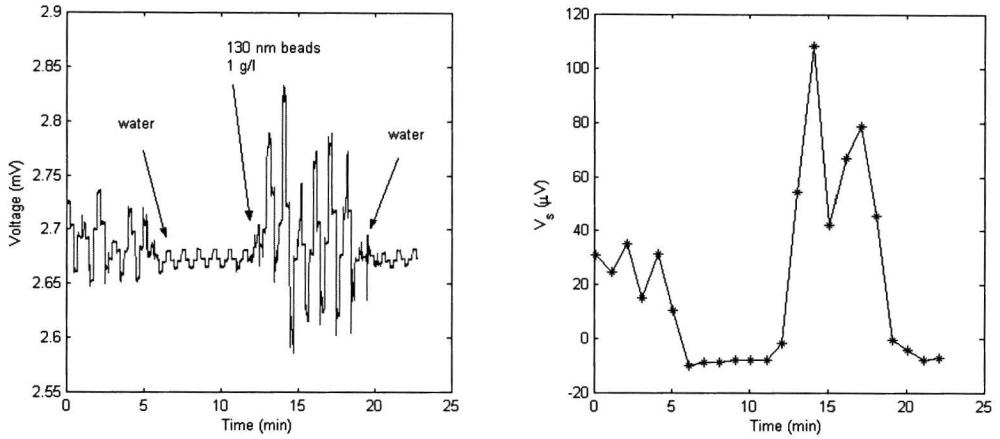

Figure A.7: Voltage versus time and signal voltage versus time of experiment 7.

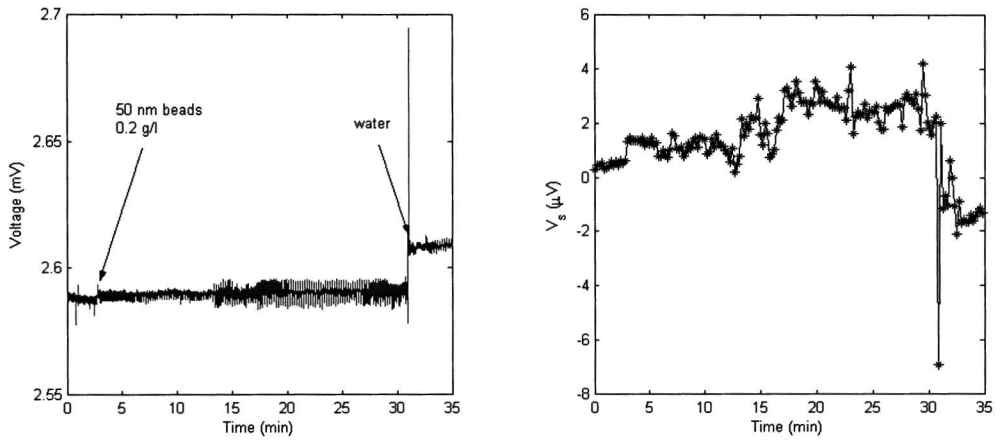

Figure A.8: Voltage versus time and signal voltage versus time of experiment 8.

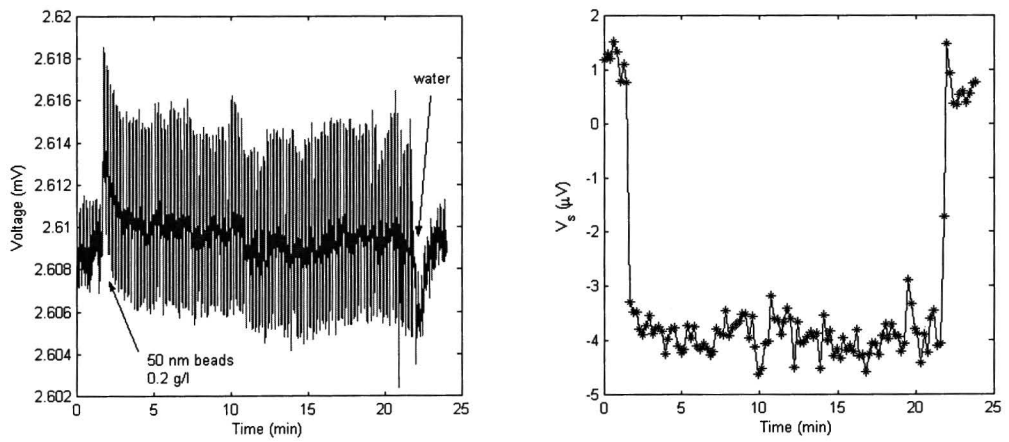

Figure A.9: Voltage versus time and signal voltage versus time of experiment 9.

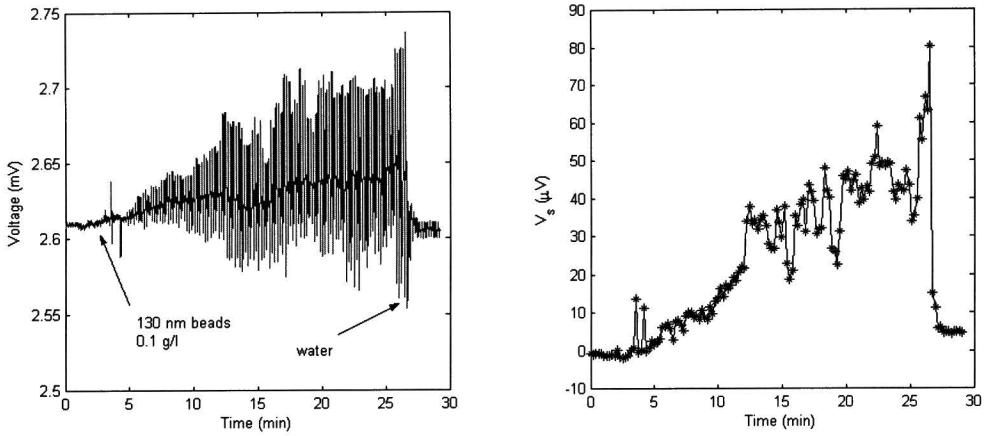

Figure A.10: Voltage versus time and signal voltage versus time of experiment 10.

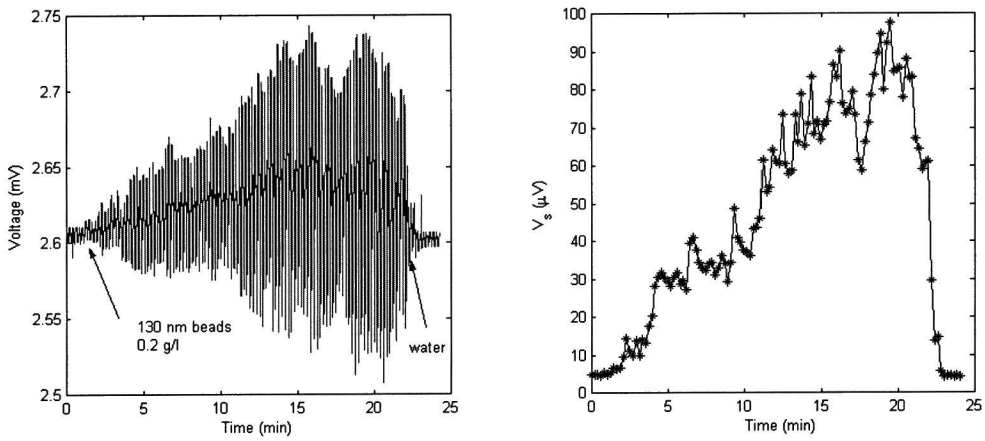

Figure A.11: Voltage versus time and signal voltage versus time of experiment 11.

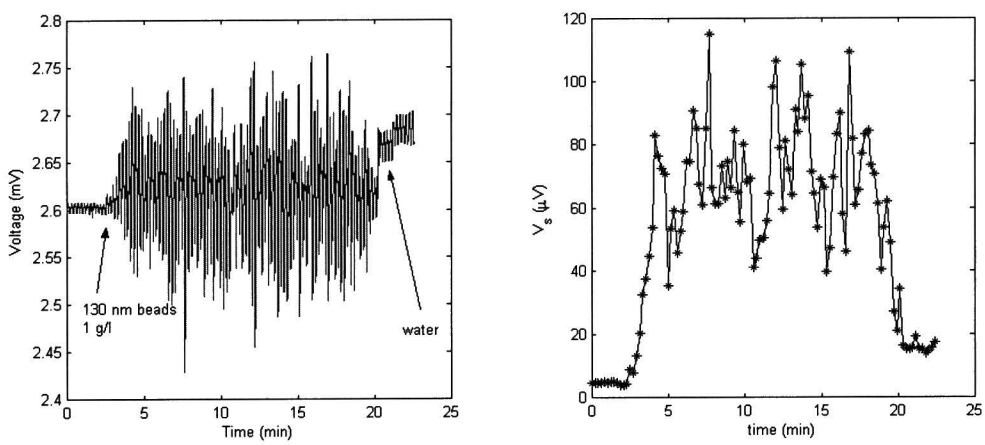

Figure A.12: Voltage versus time and signal voltage versus time of experiment 12.

B GMR resistance versus magnetic field for different alignment angles

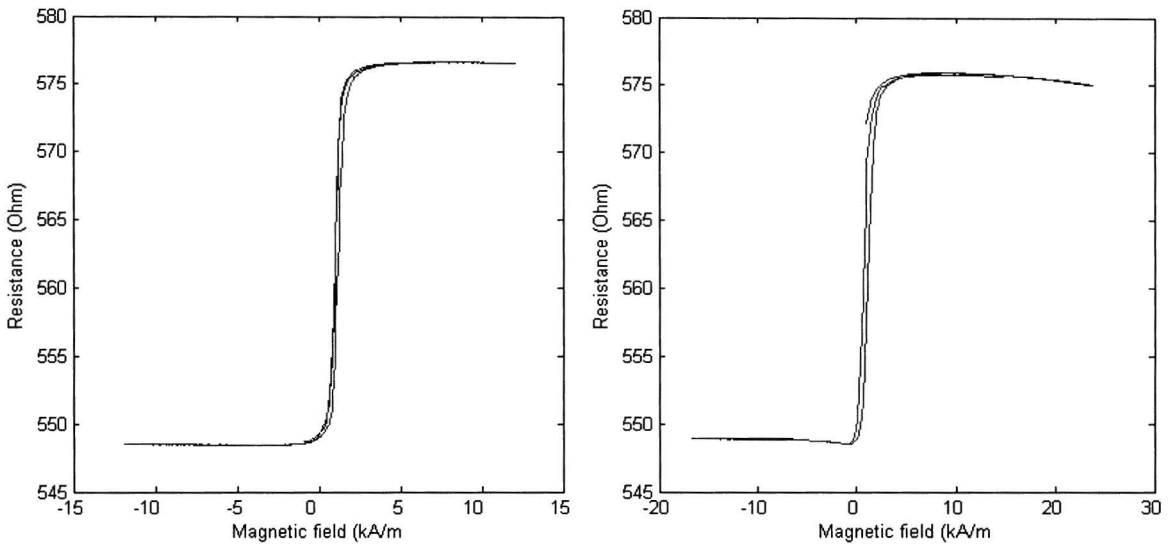

Figure B.1: Resistance versus magnetic field, on the right for zero degrees, on the left for 10 degrees.

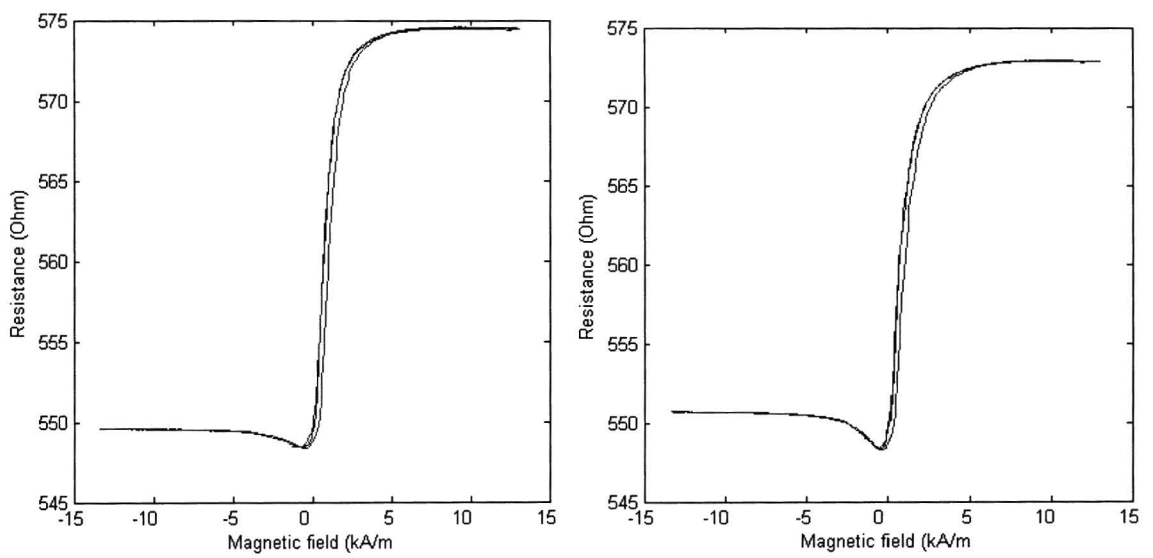

Figure B.2: Resistance versus magnetic field, on the right for 20 degrees, on the left for 30 degrees.

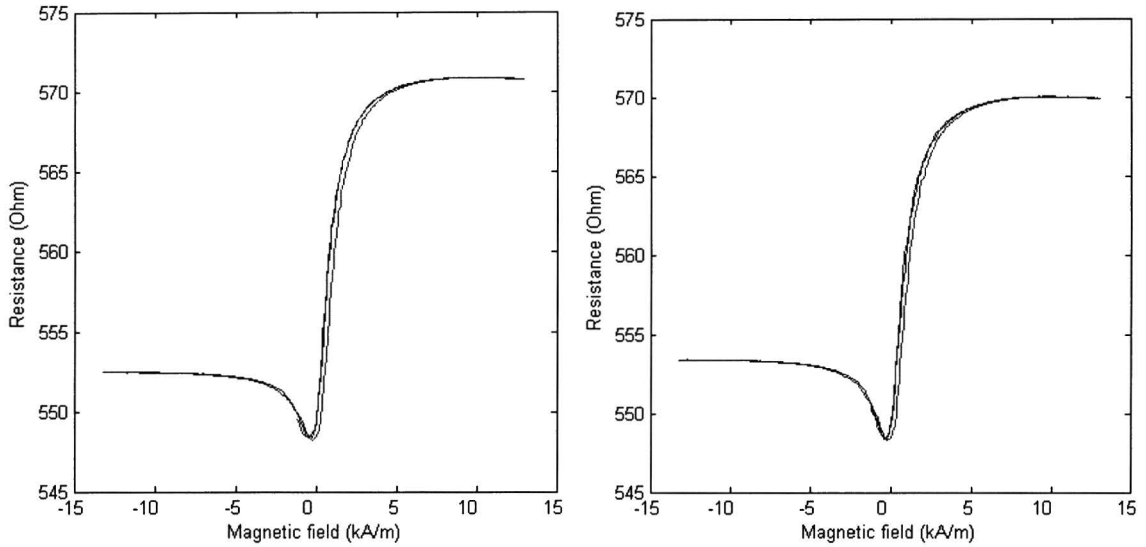

Figure B.3: Resistance versus magnetic field, on the right for 40 degrees, on the left for 45 degrees.

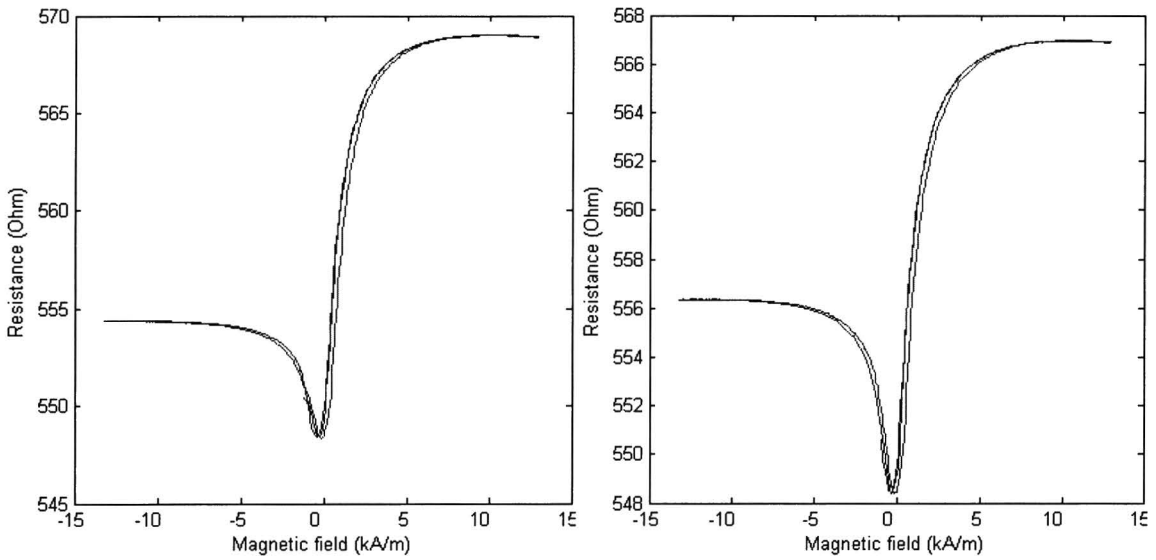

Figure B.4: Resistance versus magnetic field, on the right for 50 degrees, on the left for 60 degrees.

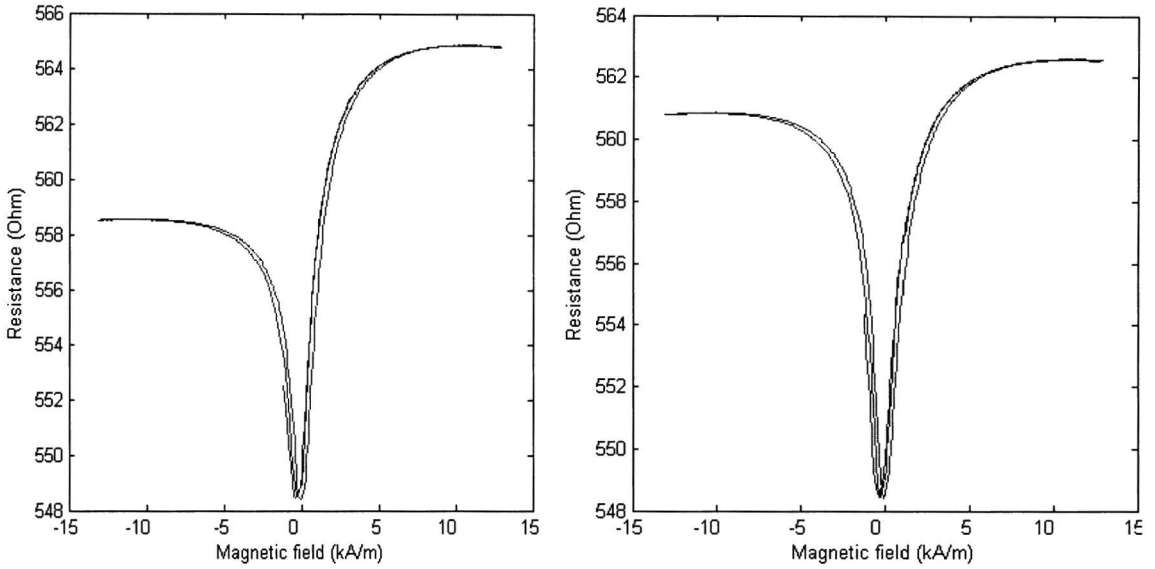

Figure B.5: Resistance versus magnetic field, on the right for 70 degrees, on the left for 80 degrees.

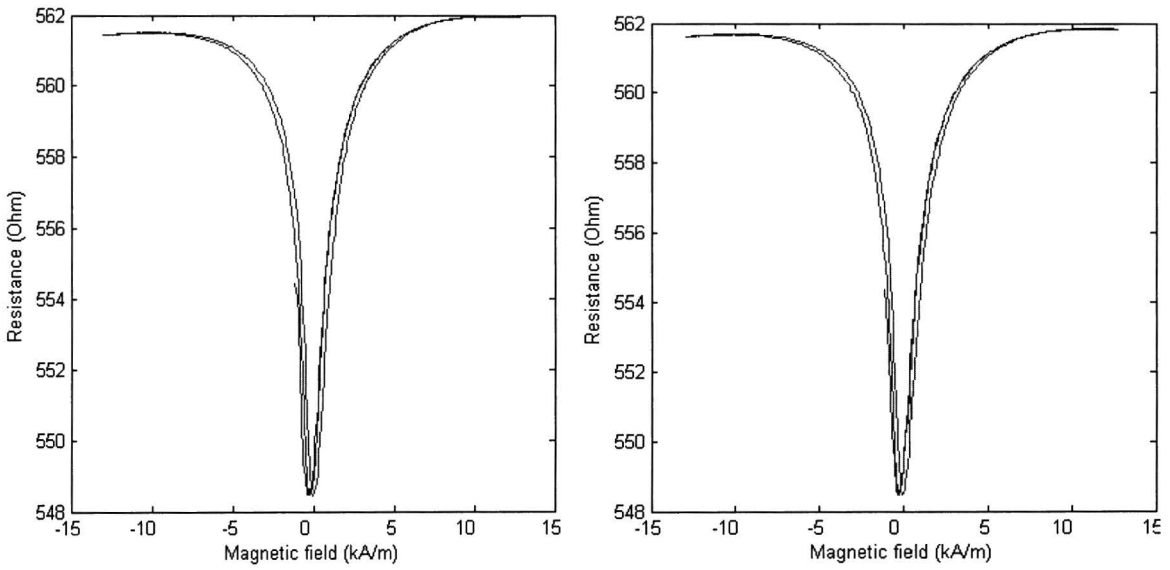

Figure B.6: Resistance versus magnetic field, on the right for 83 degrees, on the left for 84 degrees.

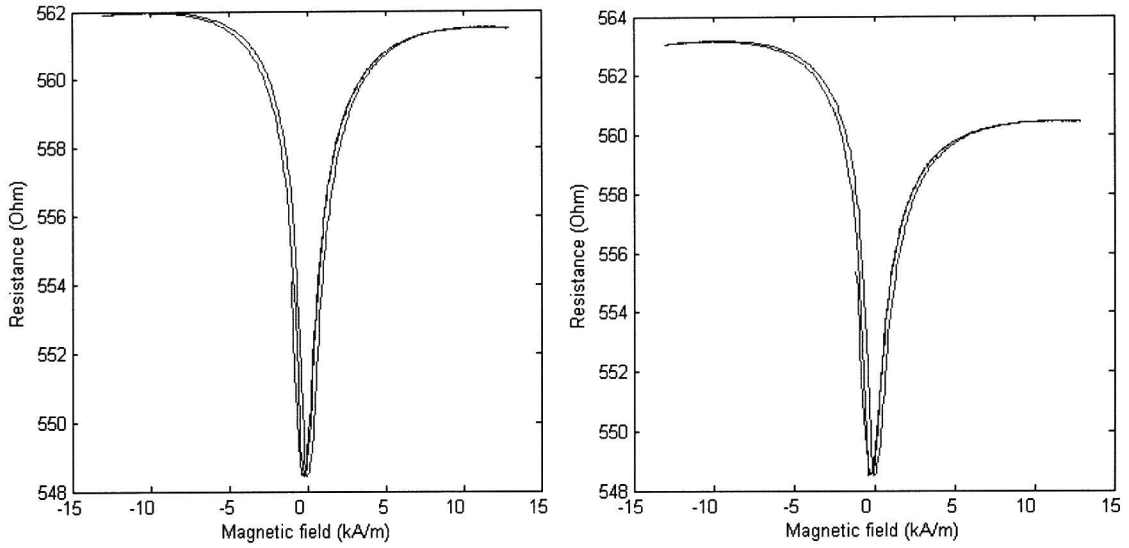

Figure B.7: Resistance versus magnetic field, on the right for 85 degrees, on the left for 90 degrees.

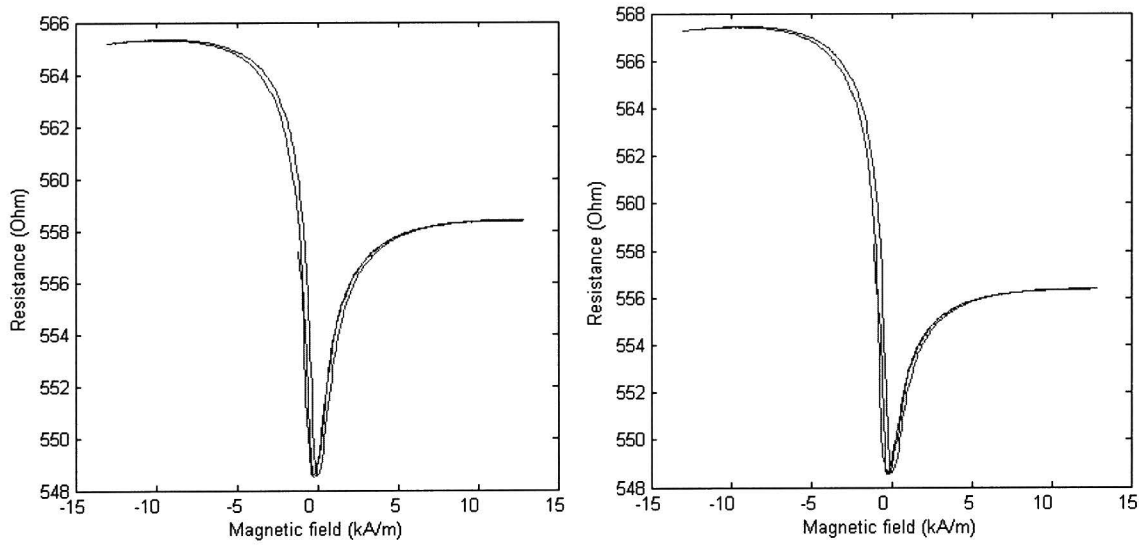

Figure B.8: Resistance versus magnetic field, on the right for 100 degrees, on the left for 110 degrees.

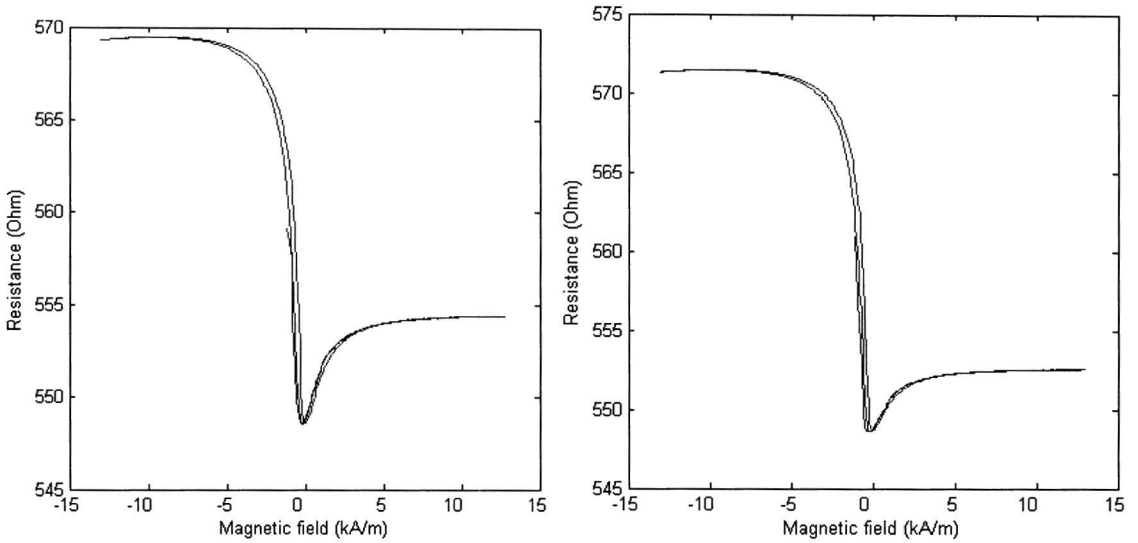

Figure B.9: Resistance versus magnetic field, on the right for 120 degrees, on the left for 130 degrees.

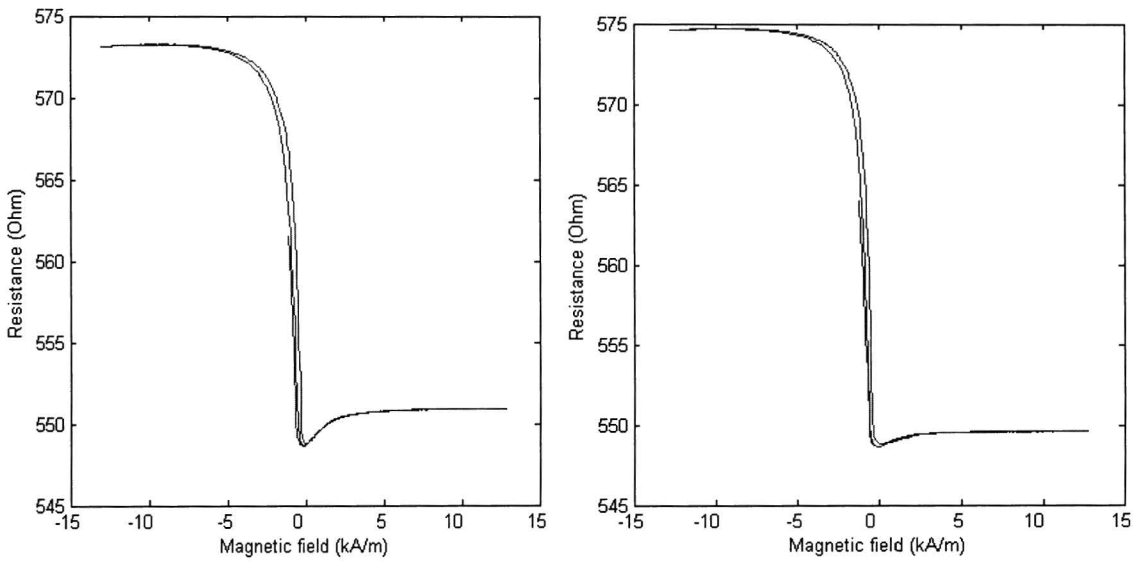

Figure B.10: Resistance versus magnetic field, on the right for 140 degrees, on the left for 150 degrees.

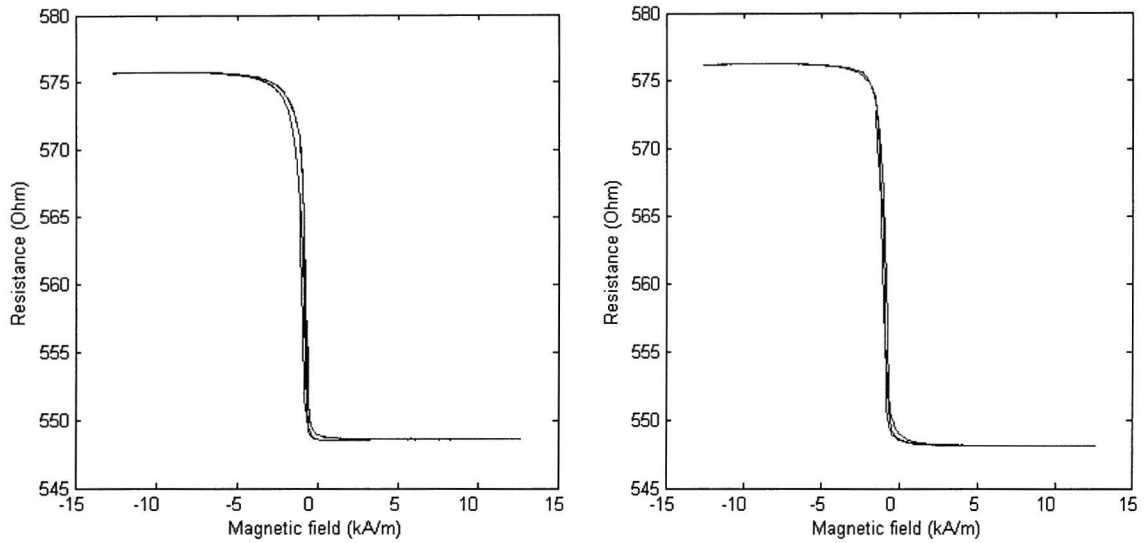

Figure B.11: Resistance versus magnetic field, on the right for 160 degrees, on the left or 170 degrees.

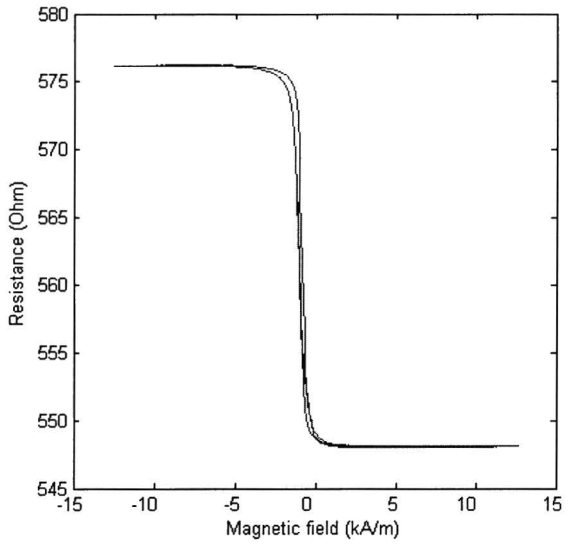

Figure B.12: Resistance versus magnetic field 180 degrees turned.

C Flow chart of chip fabrication proces

Si substrates, 0.5 μm thermal oxide, 40 x 40 mm^2

GMR Stack :

3.5 nm Ta / 2nm $Ni_{80}Fe_{20}$ / 10 nm $Ir_{20}Mn_{80}$ / 4.5 nm $Co_{90}Fe_{10}$ / 0.8 nm Ru

----------buffer----------/----------AF/AAF----------

/ 4 nm $Co_{90}Fe_{10}$ / 3nm Cu / 0.5 nm $Co_{90}Fe_{10}$ / 6 nm $Ni_{80}Fe_{20}$ / 10 nm Ta

----------/--------spacer----------/free mag. Layer/---cover----

Deposition of GMR layer, PVD (ION TECH)

Deposition of Mo hard mask layer, 6 min, PVD (JELTO)

Resist AZ4533, diluted, 5000 rpm, 10 min 90°C

Exposure mask BIOMAG1-GMR, 10 units

Development AZ developer 1:1, 3 x 20 secs

Hotplate 10 min 120 °C

Barrel etcher, 5 min O_2 plasma

Wet chemical etching of Mo, 11 secs

US acetone 3 x 2 min, resist removal

Sputter etching, 16 min, 100 Watt, 35 sccm Ar (JELTO)

Measurement of GMR effect on test structures

Sputteretching 0.5 min, 35 sccm Ar

Deposition of Mo (10 nm), 1 min, PVD (JELTO)

Deposition of Au (250 nm), 7.5 min, PVD (JELTO)

Deposition of Cr (100 nm), 2 min, PVD (NORDIKO)

Resist AZ4533, diluted, 5000 rpm, 10 min 90°C

Exposure mask BIOMAG1-OVL, 10 units

Development AZ developer 1:1, 3 x 20 sec

Hotplate 6 min 120 °C

Barrel etcher, 5 min O_2 plasma

Wet chemical etching of Cr, 6-8 min, until Au is visible

US acetone 3 x 2 min, resist removal

Sputteretching Ar/O_2, 10+12 min, 100 Watt

Sputteretching Ar, 5-6 min, 100 Watt

Deposition of SiN, 175 °C, PECVD, 0.5 µm

Sputteretching 0.5 min, 35 sccm Ar

Deposition of Mo (10 nm), 1 min, PVD (JELTO)

Deposition of Au (80 nm), 2 min 40 secs, PVD (JELTO)

Deposition of Cr (100 nm), 2 min, PVD (NORDIKO)

Resist AZ4533, diluted, 5000 rpm, 10 min 90°C

Exposure mask BIOMAG1-ACT, 10 units

Development AZ developer 1:1, 3 x 20 sec

Hotplate 6 min 120 °C

Barrel etcher, 5 min O_2 plasma

Wet chemical etching of Cr, 6-8 min, until Au is visisble

US acetone 3 x 2 min, resist removal

Sputteretching Ar/O_2, 4+3 min, 100 Watt

Sputteretching Ar, 6 min, 100 Watt

Deposition of SiN, 175 °C, PECVD, 3 .0 µm

Deposition of Cr (150 nm), 3 min, PVD (NORDIKO)

Resist AZ4533, diluted, 5000 rpm, 10 min 90°C

Exposure mask BIOMAG1-BPE, 10 units

Development AZ developer 1:1, 3 x 20 sec

Hotplate 1 min 120 °C

Barrel etcher, 5 min O_2 plasma

RIE etching of Cr (Cl_2, O_2)

RIE etching of SiN (CHF_3/O_2, prog. SINAN)

US acetone 3 x 2 min, resist removal

Wet chemical etching of Cr until Au is visible on bondpads.

D Estimation of detection limit

We can made an estimate of the detection limit of our sensor with three modifications. We make our sensor 1000 μm long instead of 100 μm, we have a GMR stack that is 4 times more sensitive, and a magnetic field of 80 kA/m. We assume that a signal voltage (2.15) of 1 μV give us a sufficient SNR.

$$V_s = 10^{-6} V = I\, s_{GMR}\, H_{x,av} = 10^{-3} * 200 \cdot 10^{-3} H_{x,av} \qquad \text{(D.1)}$$

We take a current, I, of 1 mA and a sensitivity, s, of $200 \cdot 10^{-3}$ Ωm/A. Then (2.11)

$$H_{x,av} = \frac{2mn}{\pi w} \arctan\left(\frac{w}{2t_1}\right) = \frac{2 \cdot 10^{-16} * n}{\pi 3 \cdot 10^{-6}} \arctan(3) = 2.65 \cdot 10^{-11}\, n, \qquad \text{(D.2)}$$

using a magnetic moment of the beads that equal 10^{-16} Am^2. The minimum area density of particle that can be detected is then

$$n_{\min,s} = 1.9 \cdot 10^{8} \text{ particles}/\text{m}^2 = 1.9 \cdot 10^{-4} \text{ particles}/\mu\text{m}^2 \qquad \text{(D.3)}$$

If we suppose that the area density of antibody $[Ab]$ = 1000 per μm^2, the detection limit is given by

$$f_{\min} = \frac{1}{\frac{1}{K_{eq}[Ag]} + 1} \cong \frac{n_{\min,s}}{[Ab]} = 2 \cdot 10^{-7} \qquad \text{(D.4)}$$

where f is defined as in (2.3) and K_{eq} = 10^{12} l/mol, the minimum detectable volume concentration of antigen is then

$$[Ag] = 2 \cdot 10^{-19} \text{ mol/l} \qquad \text{(D.5)}$$

Note that this is the minimum detection concentration after equilibrium has been reached, in other words after long equilibration time.

The detection limit $n_{min,b}$ for the bulk concentration as obtained when using a stepped-shaped sensor surface, without antibodies can be derived using (2.13)

$$H_{x,av} = 4.815 \cdot 10^{-17}\, n_{\min,b}. \qquad \text{(D.6)}$$

Using (D.1) we can calculate $n_{min,b}$:

$$n_{\min,b} = 1.0 \cdot 10^{-4} \text{ particles}/\mu\text{m}^3 = 1.0 \cdot 10^{-4} \text{ particles}/\mu\text{m}^3 = 0.17 \text{ pmol/l} \qquad \text{(D.7)}$$

Comparing D.5 with D.7 we see that the surface method has a potential to be much more sensitive. The advantage of the bulk method is that the detection is almost instantaneous.

Acknowledgements

I want to thank my parents, family and friends who supported me during my studies, financially as well as morally, where this report is the final assignment.

I also want to thank Dr.Ir Menno Prins and Prof.Dr. Reinder Coehoorn who were my supervisors, the people of the biosensor group: Dr. Mischa Megens, Dr.Ir. Holger Grüll, Dr. Henk Stapert, Dr.Ir. Joke Orsel, Rachel Thilwind, Jens Ruig, Ing. Ties van Bommel, Ing. Joost Kahlman, the service departments who had a lot of work with me, Dr.Ir. Hans van Zon who was in charge of the fabrication project, my roommates at Philips Research and everybody who helped me and made my live pleasant!

